

Review

Ranking Bacteria for Carbon Capture and Self-Healing in Concrete: Performance, Encapsulation, and Sustainability

Ajitanshu Vedrtam ^{1,2,*} , Kishor Kalauni ^{1,2}  and Martin T. Palou ¹ 
¹ Institute of Construction and Architecture, Slovak Academy of Science, 84503 Bratislava, Slovakia; kishor.kalauni@gmail.com (K.K.); martin.palou@savba.sk (M.T.P.)

² Department of Mechanical Engineering, Invertis University, Bareilly 243001, UP, India

* Correspondence: ajitanshu.m@invertis.org or ajitanshu.vedrtam@savba.sk

Abstract: Concrete production contributes nearly 8% of the global CO₂ emissions, making carbon capture in construction materials a critical environmental priority. While microbial self-healing concrete has shown promise in repairing structural cracks, its potential to serve as a carbon-negative material through atmospheric CO₂ sequestration remains underutilized. This interdisciplinary review—designed for materials scientists, civil engineers, and environmental technologists—systematically evaluates bacterial candidates for their application in self-healing, carbon-capturing concrete. Bacteria are ranked according to their efficiency in capturing CO₂ through both direct mechanisms (e.g., photosynthetic fixation by cyanobacteria) and indirect pathways (e.g., ureolysis-driven calcium carbonate precipitation). The assessment also considers microbial survivability in high-alkalinity concrete environments, the effectiveness of encapsulation strategies in enhancing bacterial viability and function over time, and sustainability metrics such as those derived from life cycle assessment (LCA) analyses. The findings highlight *Bacillus sphaericus* and *Sporosarcina pasteurii* as high-performing species in terms of rapid mineralization and durability, while encapsulation significantly improves the long-term viability for species like *Paenibacillus mucilaginosus* and *Synechococcus*. Notably, *Bacillus sphaericus* and *Sporosarcina pasteurii* exhibit carbonate precipitation rates of 75–100 mg CaCO₃/g biomass and enable crack closure of up to 0.97 mm within 8 weeks. The proposed bacterial ranking framework, paired with performance data and environmental modeling, provides a foundation for the advancement of scalable, carbon-negative concrete solutions.



Academic Editor: José Ignacio Alvarez

Received: 19 April 2025

Revised: 1 June 2025

Accepted: 5 June 2025

Published: 10 June 2025

Citation: Vedrtam, A.; Kalauni, K.; Palou, M.T. Ranking Bacteria for Carbon Capture and Self-Healing in Concrete: Performance, Encapsulation, and Sustainability. *Sustainability* **2025**, *17*, 5353. <https://doi.org/10.3390/su17125353>

Copyright: © 2025 by the authors. Licensee MDPI, Basel, Switzerland. This article is an open access article distributed under the terms and conditions of the Creative Commons Attribution (CC BY) license (<https://creativecommons.org/licenses/by/4.0/>).

Keywords: carbon capture; self-healing concrete; bacterial encapsulation; sustainability; life cycle assessment (LCA)

1. Introduction

Concrete is the most widely used construction material, with global production exceeding four billion tons annually. However, its high carbon footprint, contributing nearly 8% of the total anthropogenic CO₂ emissions, poses a major sustainability challenge [1,2]. Additionally, concrete's inherent brittleness and susceptibility to cracking reduce the structural lifespan, leading to frequent maintenance, increased resource consumption, and additional CO₂ emissions from repairs [3]. Self-healing concrete, an innovative bioengineered material, has emerged as a promising solution to enhance durability and reduce environmental impacts [4–7]. By embedding bacteria capable of calcium carbonate (CaCO₃) precipitation, cracks can be autonomously sealed, thereby extending the service lives of concrete structures and minimizing the need for repairs [5,8–10]. Beyond self-healing, certain bacterial species play a crucial role in carbon capture, helping to mitigate emissions from the cement

industry [11]. However, not all bacteria perform equally well, necessitating a comprehensive evaluation of their efficiency, survival, and scalability in concrete environments. The primary mechanism behind bacterial self-healing in concrete is microbially induced calcium carbonate precipitation (MICP), where bacterial metabolism facilitates the formation of CaCO_3 within cracks, sealing them and restoring the structural integrity [12–14]. This process can occur through ureolysis (urease-driven carbonate formation) or organic acid metabolism, depending on the bacterial species [8,15,16].

A comparative evaluation of microbial self-healing concrete across different bacterial strains and encapsulation techniques reveals notable improvements in compressive strength, contingent upon the microbial type, carrier method, and curing duration. Ahmad et al. [10] demonstrated that, while the inclusion of LECA-immobilized bacterial spores initially led to a modest reduction in compressive strength due to the porous nature of the aggregates, the strength recovery post-healing was significantly higher than in control mixes, particularly with *Bacillus megaterium*, which achieved superior calcite precipitation and structural integrity over a 28-day healing cycle. In contrast, Yamasmit et al. [17] observed that mortar specimens embedded with *Bacillus subtilis* microcapsules outperformed standard mortar in both early (7-day) and later (28-day) compressive strength tests. Under water curing, the compressive strength increased from 45.1 MPa in the control to 49.1 MPa in biomortar, indicating enhanced matrix densification from MICP activity. Similarly, Islam et al. [18] reported that microbial concrete incorporating *Escherichia coli* exhibited the highest compressive strength when prepared with a 50:50 water-to-bacteria mix ratio, consistently outperforming both 75:25 and control specimens across all curing periods, including long-term intervals of up to 365 days. The authors attributed this sustained strength gain to efficient bacterial colonization and internal crack bridging by CaCO_3 deposits. Collectively, these findings underscore that, while the compressive strength is influenced by both the bacterial species and carrier mechanisms, optimized MICP systems—especially those with adequate nutrient delivery and encapsulation—can reinforce the mechanical performance beyond conventional concrete benchmarks.

In addition to self-healing, certain bacteria exhibit carbon capture capabilities, either by direct CO_2 fixation, as seen in cyanobacteria [19,20], or indirect mineralization [21], as observed in ureolytic bacteria like *Sporosarcina pasteurii* [22] and *Bacillus sphaericus* [23]. These mechanisms contribute to reducing concrete's net carbon footprint, offering a potential pathway toward carbon-negative construction materials. However, the bacterial efficiency in CO_2 sequestration, their survivability in concrete's harsh alkaline conditions (pH ~12–13), and their industrial applicability vary significantly. Studies show that the MICP efficiency decreases sharply above pH 11 and that vaterite may form below pH 8, while only calcite is produced at higher pH levels [24]. To protect bacteria from alkali stress and mechanical damage during mixing, various carriers and encapsulation strategies have been developed, including organic polymers (e.g., polyurethane foams), porous lightweight aggregates, microcapsules, diatomaceous earth, alginate hydrogels, and recycled concrete aggregates coated with sodium silicate [24–26]. The concept of harnessing dormant bacterial spores to autonomously repair cracks in concrete has emerged as a powerful strategy to extend its service life. In these systems, endospores (most commonly from *Bacillus* spp.) and a suitable nutrient and calcium source are co-embedded in the cement matrix; upon crack formation, the ingress of water and oxygen triggers spore germination and metabolic activity, leading to in situ calcium carbonate (CaCO_3) precipitation that seals fissures [27,28]. Early pioneering work demonstrated up to 100 μm crack closure without external intervention, and subsequent studies have optimized factors such as the spore concentration, nutrient dosage, and curing conditions to maximize the healing efficiency [27,29].

Despite growing interest in microbial self-healing concrete, comprehensive evaluations of bacterial candidates, particularly in terms of their carbon capture potential and long-term viability, are still lacking. Although ureolytic strains such as *Sporosarcina pasteurii* and *Bacillus megaterium* can hydrolyze urea into carbonate ions (a process that is up to 10^{14} times faster than abiotic precipitation), and alternative routes like denitrification or carbonic anhydrase-mediated hydration offer further diversification for biogenic CaCO_3 formation [25,26], we still lack comprehensive evaluations regarding which bacterial candidates deliver the greatest carbon capture potential without compromising long-term viability in concrete environments.

Additionally, to quantify the environmental trade-offs of bioconcrete, several cradle-to-gate life cycle assessments (LCAs) have been conducted comparing conventional alkali-activated binders and bacterial concrete systems. Studies report that, while bacterial additives (e.g., urea, calcium salts, carrier materials) introduce embodied impacts, these can be offset by reduced repair cycles, lower CO_2 emissions via biogenic carbonation, and extended service lives [30,31]. Similarly, geopolymer- and alkali-activated concretes with MICP agents exhibit up to 30–50% lower global warming potential than OPC systems, although the impacts in categories such as eutrophication and toxicity depend sensitively on nutrient sourcing and carrier production [32]. Integrating LCA with performance data provides a comprehensive sustainability framework to guide the design of next-generation biocementitious materials.

This review aims to answer the following key question: Which bacterium is the most efficient for carbon capture and self-healing in concrete, and why? To address this, bacterial species are systematically compared based on their carbon capture mechanisms, crack healing abilities, survival and viability in concrete, industrial scalability, and effectiveness with encapsulation. The assessment includes direct versus indirect CO_2 fixation methods, CaCO_3 precipitation rates, pH resistance, spore formation, ease of cultivation, safety, and integration into concrete mixtures. Encapsulation techniques like hydrogels, lightweight aggregates (LWAs), and polymer coatings are also evaluated for their impacts on bacterial performance and feasibility. However, despite various studies on bacterial species for self-healing and carbon capture in concrete, significant research gaps persist. Most studies have focused on individual strains, without comparing multiple species under standardized criteria. The effects of encapsulation on bacterial viability and ranking are not fully understood, and the CO_2 capture potential and environmental benefits of bacterial concrete are rarely quantified. Moreover, the trade-off between crack healing and carbon capture efficiency remains unresolved, lacking an optimized solution that effectively balances both functions. This review systematically explores these factors, proposes a revised bacterial ranking, and integrates LCA to assess the sustainability of bacterial self-healing concrete, offering insights for future research and implementation in sustainable construction.

2. Direct and Indirect CO_2 Sequestration

Figure 1 illustrates the process of CO_2 sequestration, highlighting both direct and indirect methods. The left panel illustrates direct sequestration by *Synechococcus* through light-driven photosynthesis (Calvin cycle), converting CO_2 into biomass—a temporary carbon sink requiring harvest. The right panel shows indirect sequestration involving *Bacillus Sporosarcina*, which hydrolyzes urea via urease, increasing the pH and enabling the precipitation of CaCO_3 —forming a stable geological carbon sink. Key environmental factors such as light, the pH, calcium ions, and urea inputs are indicated. The hybrid zone emphasizes combinatorial potential, highlighting distinct time scales, stability profiles, and the need for tailored deployment strategies to optimize long-term climate mitigation.

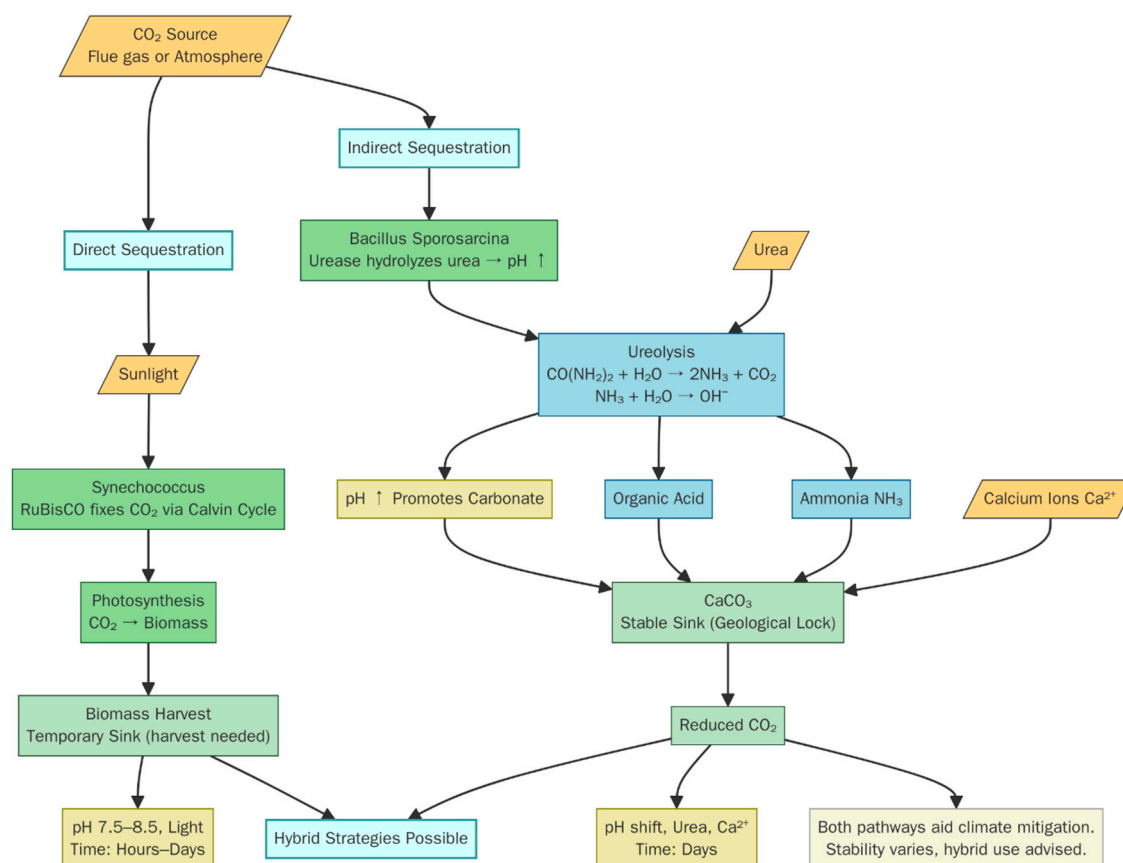


Figure 1. Integrated biological pathways for atmospheric CO₂ sequestration via direct and indirect microbial mechanisms.

Direct CO₂ fixation involves cyanobacteria, such as *Synechococcus*, capturing and converting atmospheric CO₂ into stable carbonate forms via photosynthesis-driven biomineralization [33–35]. Unlike heterotrophic bacteria, cyanobacteria actively assimilate CO₂, making them promising candidates for carbon-negative concrete applications [36,37]. *Synechococcus* facilitates CaCO₃ precipitation by raising the local pH, enabling integration into concrete while enhancing the durability and sequestering carbon. Cyanobacteria face two key challenges when incorporated into concrete. First, *Synechococcus* relies on continuous light for photosynthetic CaCO₃ precipitation, which limits its application in surface treatments or thin overlays where illumination can be guaranteed. In fully embedded or opaque sections of concrete, insufficient light penetration prevents photosynthesis and thus self-healing. Second, because cyanobacteria do not form spores, they are less resilient to extreme temperature or moisture fluctuations, compromising their long-term viability within structural concrete.

Alternative strategies include biogenic surface coatings, where *Synechococcus* biofilms on exposed concrete facilitate CO₂ capture, and translucent concrete materials that enable photosynthetic activity. However, these remain experimental, requiring further optimization for real-world scalability. Given their light dependency, cyanobacteria are more suited for biocement coatings, eco-friendly facades, or hybrid carbon-sequestering materials rather than structural concrete. Future advancements in microbial encapsulation, biofilm engineering, or material transparency may enhance their applicability in carbon-capturing construction materials.

Indirect CO₂ sequestration in concrete is driven by microbial metabolic pathways that induce CaCO₃ precipitation, thereby locking CO₂ within the cementitious matrix [38]. Unlike direct fixation by autotrophic organisms, heterotrophic bacteria, such as *Bacillus*

and *Sporosarcina*, facilitate carbonate mineralization through metabolic alkalization and carbonate ion generation [39]. The efficiency of these processes depends on the biochemical pathways, pH modulation, substrate availability, and ionic interactions within the concrete matrix. Two dominant mechanisms (ureolysis and organic acid metabolism) govern microbial carbonate precipitation, each offering distinct trade-offs in kinetic efficiency, environmental impacts, and long-term stability.

Ureolytic bacteria such as *Sporosarcina pasteurii* and *Bacillus sphaericus* hydrolyze urea via urease enzymatic activity, generating ammonia (NH_3) and carbonate [40], leading to localized alkalinity and carbonate saturation. This rapid nucleation process facilitates high-efficiency CaCO_3 precipitation, making ureolysis one of the most effective microbial pathways for biocementation. However, it also produces NH_3 emissions, posing environmental and regulatory challenges. NH_3 volatilization contributes to air pollution and nitrate accumulation, necessitating integrated NH_3 capture strategies or the development of NH_3 -limiting metabolic control systems. A major constraint in ureolytic systems is urea availability, as sustained carbonate precipitation requires a continuous supply. Encapsulation strategies involving silica aerogels, polymer microspheres, and hydrogel matrices have been explored to control substrate release and prolong bacterial viability. Despite their efficiency, ureolysis-based systems risk premature pore clogging due to rapid carbonate deposition, limiting long-term reactivation in cracked concrete.

Non-ureolytic carbonate precipitation occurs via organic acid metabolism, where bacteria such as *Bacillus pseudofirmus* and *Paenibacillus mucilaginosus* ferment organic substrates (e.g., calcium lactate oxidation) to produce bicarbonate (HCO_3^-) and CO_2 , leading to gradual pH-buffered CaCO_3 nucleation [41]. Unlike ureolysis, this pathway avoids NH_3 emissions, making it a more sustainable alternative for CO_2 sequestration in concrete applications. However, organic acid-mediated mineralization exhibits slower kinetics, requiring external carbon sources and optimized metabolic regulation to enhance the CaCO_3 yields. The efficiency of this process is influenced by the substrate availability, redox balance, and oxygen diffusion within the concrete microenvironment, making it less suitable for rapid crack healing but more effective for long-term carbonation stability. While ureolytic bacteria offer high carbonate deposition rates ($\sim 50\text{--}100\text{ mg CaCO}_3/\text{g biomass}$), they require strict NH_3 management systems. Table 1 illustrates the comparative trade-offs between ureolysis and organic acid metabolism for MICP in concrete.

Table 1. Trade-offs and optimization strategies.

Parameter	Ureolysis (Urease-Driven)	Organic Acid Metabolism (Fermentation-Driven)
Primary Bacteria	<i>Sporosarcina pasteurii</i> , <i>Bacillus sphaericus</i>	<i>Bacillus pseudofirmus</i> , <i>Paenibacillus mucilaginosus</i>
Carbonate Yield	High (fast CaCO_3 precipitation)	Moderate (slower deposition)
pH Effect	Strong pH increase (>9)	Mild pH increase
CO_2 Sequestration	Indirect (via ureolysis byproducts)	Indirect (via bicarbonate formation)
Byproducts	NH_3 emissions	CO_2 , organic acids (sustainable)
Industrial Feasibility	High (fast reaction, proven application)	Moderate (requires carbon source)
Environmental Impact	NH_3 pollution concerns	Low environmental impact

Ureolysis, primarily utilized by *Sporosarcina pasteurii* and *Bacillus sphaericus*, exhibits high carbonate yields and industrial feasibility but generates NH_3 as a byproduct, necessitating mitigation strategies. Conversely, organic acid metabolism, performed by *Paenibacillus mucilaginosus* and *Bacillus pseudofirmus*, has a higher sustainability score and lower environmental impact but produces CaCO_3 at a slower rate.

Figure 2 visually represents the relative efficiency of these metabolic pathways across key parameters, with green indicating high performance, yellow moderate, and red low. Ureolysis performs well in terms of the carbonate yield, pH effect, and industrial feasibility but has lower CO_2 sequestration, byproduct generation, and environmental impact scores compared to organic acid metabolism. Organic acid metabolism excels in terms of CO_2

sequestration, byproducts, and environmental impacts but is less favorable in terms of its carbonate yield and industrial feasibility. The chart highlights the trade-offs between the two pathways, showing that each is more suitable for different objectives.

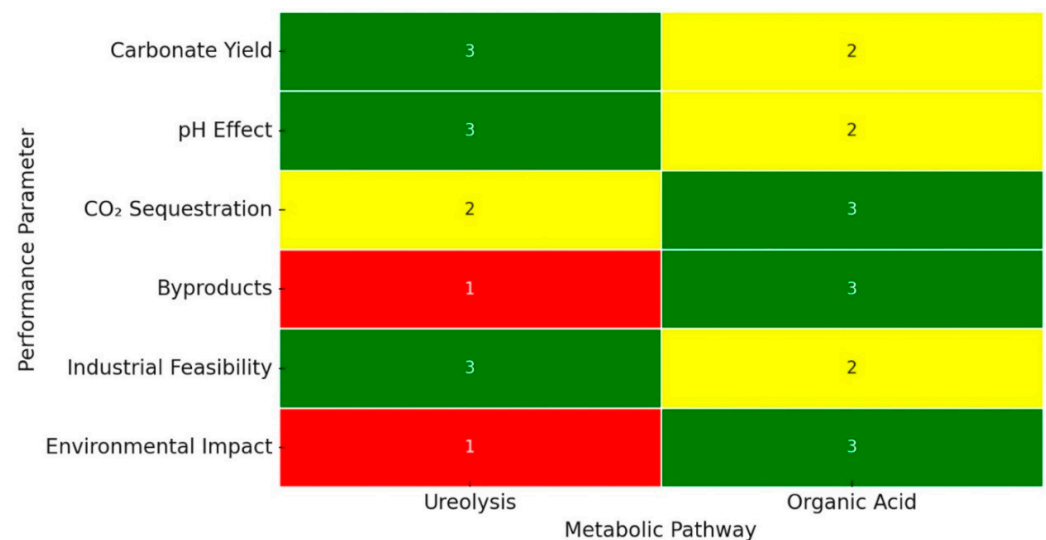


Figure 2. Trade-offs between ureolysis and organic acid metabolism (green (high), yellow (moderate), red (low)).

Figure 3 provides a quantitative comparison, demonstrating that ureolysis enables rapid biocementation but with environmental trade-offs, while organic acid metabolism supports long-term carbon sequestration with reduced byproducts. These findings highlight the necessity of hybrid microbial approaches or encapsulation techniques to optimize bacterial viability and balance fast crack healing with sustainable CO₂ sequestration in bioengineered concrete.

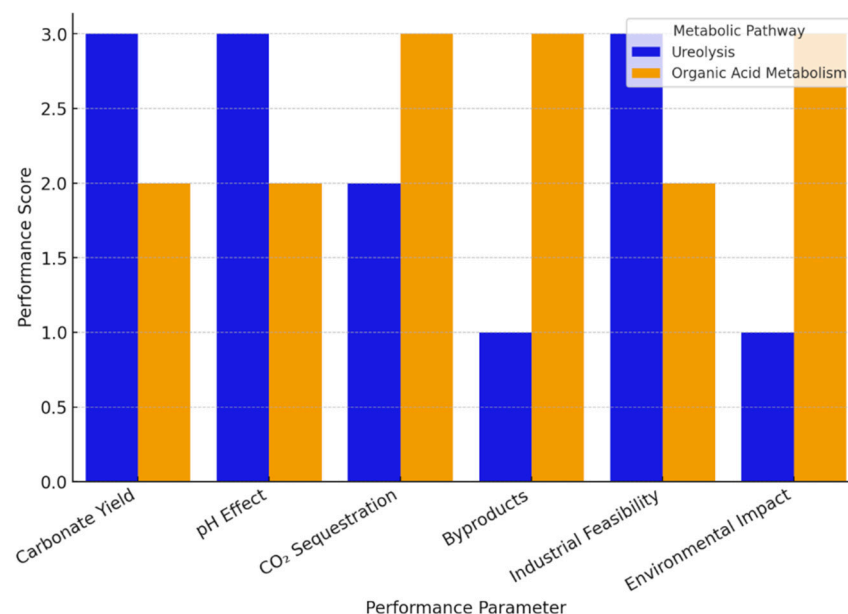


Figure 3. Comparison of ureolysis vs. organic acid metabolism.

To balance rapid initial CaCO₃ formation with long-term carbonation stability, hybrid microbial consortia incorporating ureolytic and organic acid-metabolizing bacteria have been recommended. Encapsulation in nanoporous carriers has shown promise in modulating microbial activity, ensuring controlled carbonate precipitation while minimizing NH₃

volatilization. The genetic engineering of urease regulatory pathways may further enhance the metabolic switching mechanisms, allowing for NH_3 -reducing, self-regulating biomineralization cycles within concrete matrices. The effectiveness of microbial CO_2 sequestration in concrete depends on the biomass-specific CaCO_3 precipitation rates, metabolic stability, and long-term mineralization potential. While ureolytic species like *Sporosarcina pasteurii* remain the most efficient for rapid biocementation, *Paenibacillus mucilaginosus* presents a more sustainable alternative for large-scale carbon capture applications.

2.1. Efficiency of CO_2 Sequestration Among Key Bacteria

The efficiency of microbial CO_2 sequestration in concrete depends on the rate of CaCO_3 precipitation per unit biomass and the extent to which CO_2 is permanently stored within the cementitious matrix. While both ureolytic and non-ureolytic bacteria contribute to CO_2 mineralization, their relative efficiency varies based on the precipitation kinetics, metabolic pathways, and environmental stability. Figure 4 shows the microbial pathways for atmospheric CO_2 mineralization. The diagram illustrates three primary biological mechanisms (photosynthetic fixation (purple), ureolysis pathway (yellow), and organic acid metabolism (green)) used by different microbes to precipitate CaCO_3 from atmospheric CO_2 . Each pathway varies in its rate of CaCO_3 formation, environmental impact, and byproduct output, with key microbial species and characteristics.

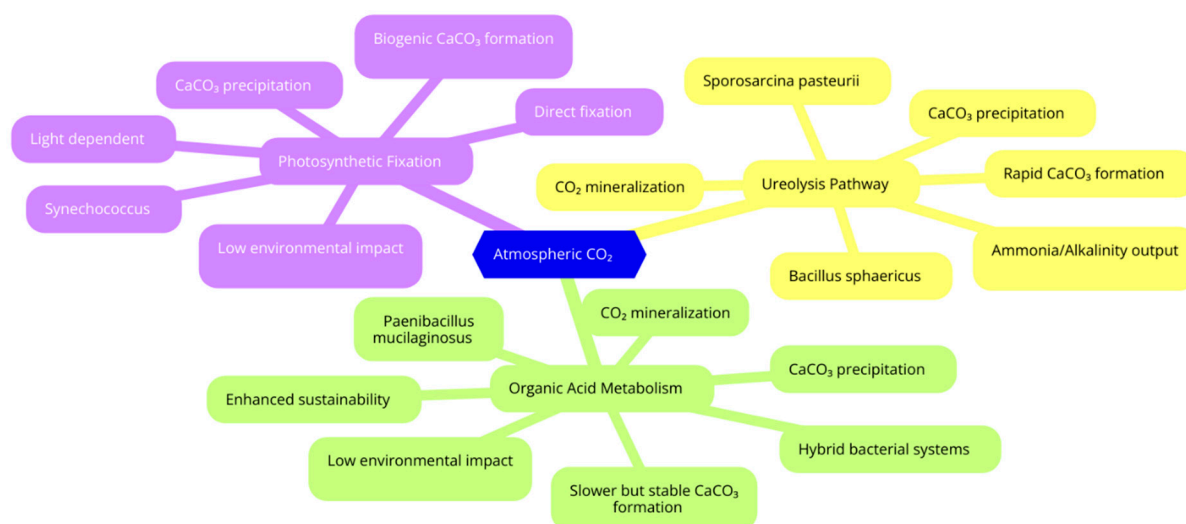


Figure 4. Microbial pathways for atmospheric CO_2 mineralization.

The Sankey diagram (Figure 5) visually represents the carbon mineralization efficiency of different bacterial pathways, showing the flow of atmospheric CO_2 through three primary sequestration mechanisms (ureolysis, organic acid metabolism, and photosynthesis). Each pathway channels CO_2 into specific bacteria, such as *Bacillus sphaericus* and *Sporosarcina pasteurii* (ureolysis), *Paenibacillus mucilaginosus* (organic acid metabolism), and *Synechococcus* (photosynthesis), which then convert it into stable CaCO_3 precipitation. The thickness of each flow corresponds to the efficiency ($\text{mg CaCO}_3/\text{g biomass}$), highlighting *Bacillus sphaericus* and *Paenibacillus mucilaginosus* as the most effective in CaCO_3 formation, while *Sporosarcina pasteurii* and *Synechococcus* exhibit the lowest efficiency. The Sankey diagram quantifies the carbon flow through three primary mechanisms: ureolysis (50%), organic acid metabolism (30%), and photosynthesis (20%). Ureolytic bacteria such as *Bacillus sphaericus* and *Sporosarcina pasteurii* contribute 40% and 10%, respectively, while *Paenibacillus mucilaginosus* via organic acid metabolism accounts for 30%. *Synechococcus*, a

photosynthetic cyanobacterium, contributes the remaining 20%. Combined, these pathways result in 89% stable calcium carbonate precipitation efficiency.

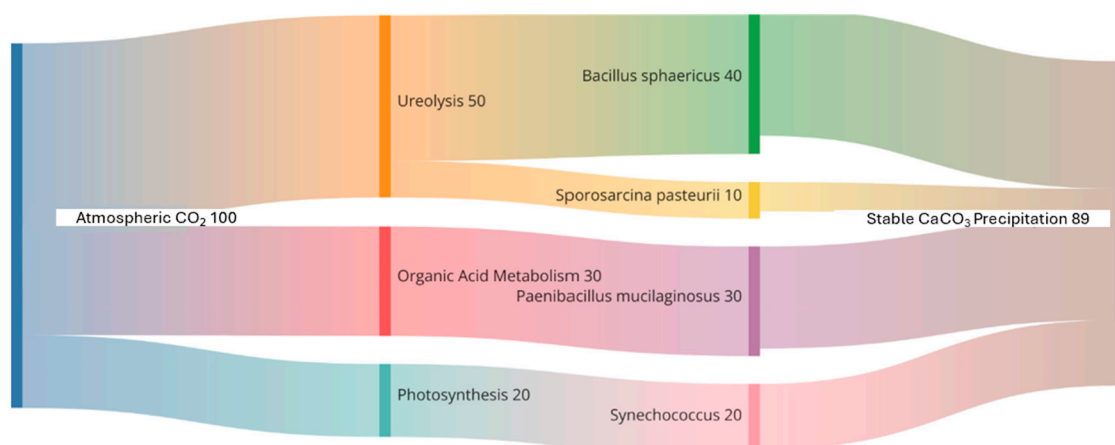


Figure 5. Sankey diagram of the carbon mineralization efficiency of different bacterial pathways to stable CaCO₃ precipitation from atmospheric CO₂.

2.2. Comparative Analysis of Carbon Mineralization Rates per Unit Biomass

The rate of microbial carbonate precipitation is governed by metabolic activity, substrate availability, and environmental conditions such as the pH and calcium ion concentration. Table 2 compares key bacteria used in concrete based on their precipitation rates, metabolic pathways, and long-term stability. Ureolytic bacteria, particularly *Sporosarcina pasteurii* and *Bacillus sphaericus*, exhibit high carbonate precipitation rates (~50–100 mg CaCO₃/g biomass) due to their ability to rapidly hydrolyze urea and generate carbonate ions. However, this comes at the cost of NH₃ release, which may require mitigation strategies to prevent environmental pollution. In contrast, non-ureolytic bacteria, such as *Bacillus pseudofirmus* and *Paenibacillus mucilaginosus*, induce slower but sustained CaCO₃ precipitation (~20–40 mg CaCO₃/g biomass) via organic acid metabolism. This pathway provides stable CO₂ sequestration over extended periods, avoiding the rapid pore clogging often observed in ureolytic systems. Additionally, these bacteria do not require urea supplementation, making them more suitable for large-scale applications where controlled nutrient supply is a challenge.

Table 2. Comparison of key bacteria used in concrete based on their precipitation rates, metabolic pathways, and long-term stability.

Bacterium	Precipitation Rate (mg CaCO ₃ /g Biomass)	Primary Mechanism	Byproducts	Long-Term Stability	Refs.
<i>Sporosarcina pasteurii</i>	80–100	Ureolysis	NH ₃	Moderate	[42]
<i>Bacillus sphaericus</i>	75–90	Ureolysis	NH ₃	Moderate	[23]
<i>Bacillus subtilis</i>	65–75	Ureolysis + Organic Acid	NH ₃ + CO ₂	Moderate–High	[43]
<i>Bacillus pseudofirmus</i>	45–55	Organic Acid Metabolism	CO ₂ , Organic Acids	High	[44]
<i>Paenibacillus mucilaginosus</i>	30–45	Organic Acid Metabolism	CO ₂ , Organic Acids	Very High	[45]
<i>Synechococcus</i> spp.	100–120	Photosynthesis	Oxygen, Carbonates	Low	[46]
<i>Bacillus megaterium</i>	55–65	Ureolysis + Organic Acid	NH ₃ + CO ₂	Moderate–High	[47]
<i>Lysinibacillus sphaericus</i>	85–95	Ureolysis	NH ₃	Moderate	[48]
<i>Pseudomonas fluorescens</i>	40–50	Organic Acid Metabolism	CO ₂ , Organic Acids	High	[49]

While ureolytic bacteria outperform non-ureolytic bacteria in terms of their short-term carbonate precipitation rates, their efficiency is often limited by substrate depletion and NH₃-related issues. Non-ureolytic species offer a more controlled and stable carbon capture pathway, making them more desirable for long-term CO₂ sequestration strategies.

The precipitation rates and performance values presented in Table 2 are drawn from individual experimental studies, each employing distinct test setups, bacterial strains,

and concrete conditions. Due to this heterogeneity, a standardized statistical comparison (e.g., ANOVA or pooled variance analysis) was not performed. Instead, the precipitation efficiency is reported as typical ranges cited in the literature to allow for qualitative interspecies comparison. Future work should aim to consolidate raw experimental data under standardized conditions, enabling a statistically rigorous meta-analysis and clearer benchmarking across microbial species. Until then, the comparative insights provided here should be interpreted as approximate rather than statistically definitive.

2.3. Influence of Bacterial Metabolism on the Extent and Permanence of CO₂ Storage

The extent of CO₂ storage in bacterial concrete is fundamentally influenced by the stability of the precipitated CaCO₃ and its resistance to dissolution over time. Although both ureolytic and organic acid-based microbial pathways facilitate carbonate mineralization, significant differences in the crystal morphology, bonding strength, and integration with the cementitious matrix determine the permanence of the sequestered carbon. Ureolytic bacteria typically generate vaterite, a metastable polymorph of CaCO₃. While effective for rapid mineralization, vaterite is prone to transformation into more stable forms such as calcite, a process that may, under certain environmental conditions, result in partial CO₂ release. In contrast, organic acid-producing bacteria tend to directly precipitate calcite, the most thermodynamically stable form of CaCO₃. This enhances long-term carbon retention by reducing the likelihood of mineral transformation or dissolution within the concrete matrix. The location of mineralization significantly affects its durability. Bacteria residing within microcracks contribute to more permanent mineral integration by promoting in situ crack healing and mechanical reinforcement. Conversely, CaCO₃ formed on surface layers is more susceptible to environmental wear and erosion, limiting its role in sustained CO₂ sequestration. Enhancing bacterial viability is essential for prolonged mineralization cycles. Encapsulation technologies, such as embedding bacteria in silica aerogels or polymeric microspheres, protect microbial cells from harsh cementitious environments and extend their metabolic activity. Without encapsulation, bacteria often lose viability shortly after concrete setting, significantly diminishing their long-term CO₂ capture capacity. While ureolytic bacteria are advantageous for rapid biocementation due to their high precipitation rates, their reliance on urea hydrolysis poses environmental challenges, including NH₃ release, and introduces risks of CO₂ re-release through unstable mineral phases. In contrast, organic acid-producing bacteria provide a more stable and sustainable route for carbon capture, albeit typically at slower rates. A promising solution lies in the development of hybrid microbial systems that combine the rapid mineralization of ureolytic species with the long-term stability offered by organic acid-based organisms.

While the current ranking framework incorporates the CO₂ capture efficiency in terms of CaCO₃ precipitation rates, it does not yet account for the polymorphic form of the precipitated mineral—specifically, the distinction between vaterite and calcite. This omission is significant, as vaterite is a metastable phase prone to dissolution or transformation under environmental stress, whereas calcite is thermodynamically stable and offers more durable carbon storage. Ureolytic bacteria, such as *Sporosarcina pasteurii*, often initiate vaterite formation, while organic acid-producing bacteria like *Paenibacillus mucilaginosus* tend to favor calcite. Incorporating a crystallographic stability coefficient or polymorph index into the ranking system could improve its predictive power regarding long-term CO₂ retention and material durability. Future iterations of the MCDA framework will integrate this factor as a performance modifier, using XRD-verified mineral data from experiments.

2.4. Finite Difference Method (FDM)

The finite difference method (FDM) is used to simulate the time-dependent healing of cracks in concrete through MICP. The FDM simulation demonstrates how MICP facilitates crack healing in concrete over time. The process begins with an initial crack region (low CaCO_3 concentration), which progressively fills as bacterial activity induces mineralization. Higher-bacterial-density zones show faster healing, while diffusion ensures even CaCO_3 deposition, effectively sealing the crack. This model confirms that MICP-based self-healing concrete can autonomously repair structural damage, enhancing the durability, longevity, and sustainability in construction materials. A 2D grid-based model (Figure 6) represents a concrete section with an initial crack region that progressively heals due to bacterial activity. The simulation considers

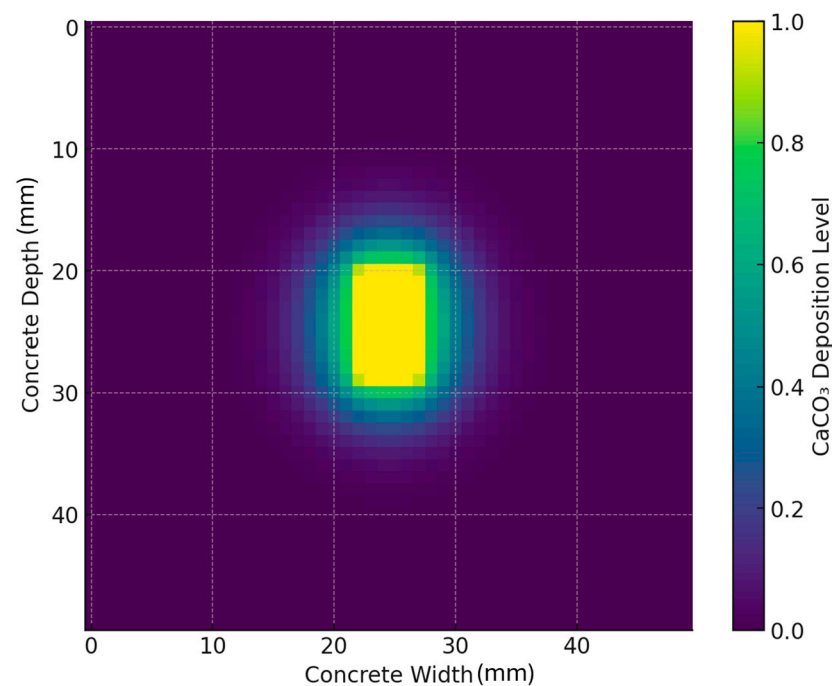


Figure 6. Finite difference method (FDM) simulation of time-dependent crack healing in concrete using MICP.

- The CaCO_3 deposition rate governed by bacterial ureolysis;
- The diffusion of calcium ions (Ca^{2+}) and carbonate ions (CO_3^{2-}) within the crack;
- The precipitation kinetics, where mineralization occurs in regions with high ion concentrations.

The healing process is modeled using the reaction–diffusion equation (Equation (1)):

$$C_{i,j}^{t+1} = C_{i,j}^t + D\nabla^2 C_{i,j}^t + R_{i,j} \cdot M_{i,j} \quad (1)$$

where $C_{i,j}^t$ represents the CaCO_3 concentration at location (i, j) and time t , $D\nabla^2 C$ is the diffusion term for calcium and carbonate ions, $R_{i,j}$ is the precipitation reaction rate (governed by bacterial metabolism), and $M_{i,j}$ represents bacterial presence, enhancing mineralization.

A 50×50 grid is used to simulate a concrete cross-section containing an initial crack, represented by an area with a zero CaCO_3 concentration. Bacterial colonies are pre-seeded throughout the matrix to induce mineralization, promoting self-healing within the concrete. Over the course of 200 iterative time steps, diffusion and precipitation processes take place, gradually increasing the CaCO_3 concentration in the cracked region until the crack is effectively sealed.

The CFD-inspired simulation models CO₂ diffusion and bacterial mineralization within a porous concrete matrix using a numerical finite difference approach to approximate the transport and reaction dynamics. A 50 × 50 computational grid represents the cross-section of a concrete slab, with CO₂ initially concentrated at the surface layer (top boundary) to simulate exposure to atmospheric CO₂. The diffusion process follows a 2D discrete Laplacian operator, where each grid cell exchanges CO₂ with its neighboring cells based on a diffusion coefficient (0.1 arbitrary units). To incorporate bacterial mineralization, regions with a higher bacterial density (predefined zones) are assigned increased sequestration rates, modeled as localized CO₂ depletion via a bacterial uptake function. The governing equation (Equation (2)) at each timestep is

$$C_{i,j}^{t+1} = C_{i,j}^t + D\nabla^2 C_{i,j}^t - M_{i,j} \cdot R \quad (2)$$

where $C_{i,j}^t$ represents the CO₂ concentration at cell (i, j) and time t ; $D\nabla^2 C$ is the diffusion term for CO₂, approximated using a 5-point stencil Laplacian; R is the CO₂ sequestration rate, set at 0.02 per unit of bacterial activity; and $M_{i,j}$ represents bacterial presence, enhancing mineralization at location (i, j) .

At each timestep, CO₂ diffusion is calculated, bacterial mineralization is subtracted, and values are constrained to remain non-negative. This iterative process simulates CO₂ transport and sequestration over 100 timesteps, providing a qualitative visualization of the bacterial efficiency in CO₂ reduction within concrete. The CFD-inspired simulation (Figure 7) visualizes CO₂ diffusion and bacterial mineralization in a porous concrete matrix, showing how bacterial activity enhances localized CO₂ sequestration. The simulation is based on a simplified finite difference (FD) approximation of Fick's second law to represent 2D CO₂ diffusion and microbially induced mineralization in a porous concrete matrix. The domain is discretized into a 50 × 50 grid, where each cell represents a 1 mm² section of the concrete cross-section. CO₂ concentration is initialized at the top boundary (surface exposure) to simulate contact with the atmosphere, while bacterial activity is spatially distributed across the grid as predefined zones with higher uptake rates.

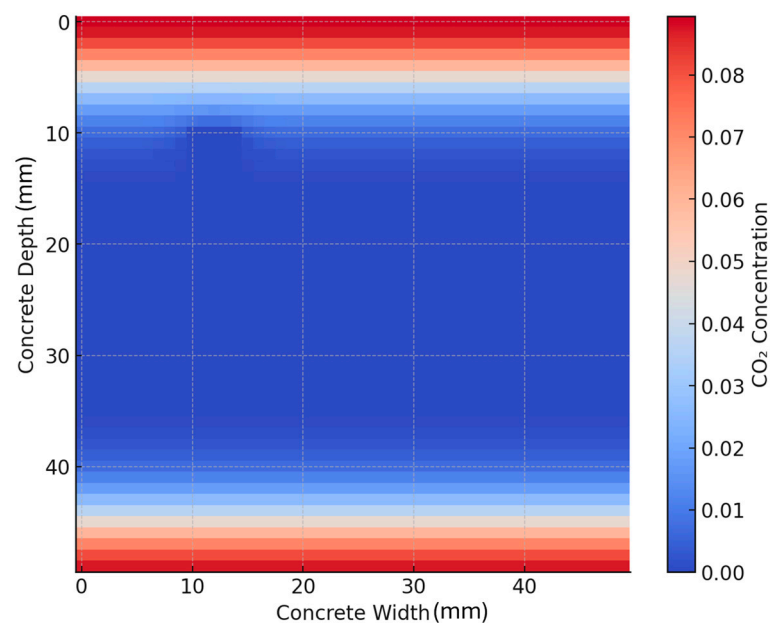


Figure 7. CO₂ diffusion and mineralization in concrete (CFD approximation).

The governing equation at each grid point (i, j) and time step t is

$$C_{i,j}^{t+1} = C_{i,j}^t + D\Delta C_{i,j} - B_{i,j} \cdot R$$

where $C_{i,j}$ is the local CO₂ concentration, D is the diffusion coefficient (set to 0.1 for normalized simulation units), $\Delta(C)_{i,j}$ is the discrete Laplacian (5-point stencil), R is the bacterial mineralization rate (0.02 per time step per active cell), and $B_{i,j}$ is a binary mask representing bacterial presence (1 if active, 0 otherwise).

The boundary conditions are zero flux (Neumann) on the sides and a fixed CO₂ concentration on the top boundary. The simulation is run for 100 iterations, and color gradients represent decreasing CO₂ concentrations due to bacterial sequestration over time.

Although this is not a full Navier–Stokes-based CFD model, it serves as a valid reaction–diffusion approximation for the visualization of the interplay between gas transport and localized microbial activity in static porous media. The aim is to illustrate the qualitative spatial effects of microbial distribution and encapsulation zones on CO₂ reduction, rather than predict exact field values.

The highest CO₂ concentrations appear near the exposed surface, gradually diffusing into the material, while regions with a greater bacterial presence exhibit lower CO₂ levels, indicating active mineralization. This confirms that bacterial self-healing concrete can effectively capture and convert CO₂, reinforcing its potential as a carbon-negative construction material for sustainable infrastructure.

Although the FDM- and CFD-inspired simulations provide mechanistic insights into CO₂ diffusion and bacterial CaCO₃ precipitation, they currently serve as qualitative models due to the lack of access to standardized, high-resolution experimental datasets for calibration. Key parameters such as the ion diffusion coefficients within cementitious matrices, in situ CO₂ mineralization rates under varying encapsulation conditions, and time-resolved crack healing profiles (mm/day) are either sparsely reported or vary widely across studies. As such, model validation using RMSE analysis or parameter optimization is presently constrained by poor data availability. Future work will aim to generate or access harmonized lab-scale datasets—particularly for the bacterial activity profiles and CaCO₃ deposition kinetics under defined environmental conditions—to transition these simulations from illustrative frameworks to predictive field-relevant tools.

3. Ranking Bacteria for Self-Healing Carbon-Capturing Concrete

To identify the optimal bacterial strains for use in self-healing, carbon-sequestering concrete, each candidate is systematically evaluated against four key criteria, each assigned a specific weight based on its relative importance. The most critical factor is the carbon capture efficiency (40%), which measures the bacterium's ability to convert CO₂ into stable carbonate minerals, such as CaCO₃, per unit of biomass. This includes both autotrophic CO₂ fixation, as seen in photosynthetic organisms, and heterotrophic precipitation via metabolic byproducts, such as urea hydrolysis or organic acid production. Higher scores in this category reflect greater mineral yields and CO₂ sequestration capabilities. The second criterion, survival in concrete (30%), assesses the organism's resilience within the harsh concrete environment, which is characterized by high alkalinity (pH ~12–13), prolonged dryness, and nutrient scarcity. Spore-forming alkaliphilic bacteria receive the highest scores due to their ability to endure these extreme conditions by entering a dormant state until favorable conditions return. In contrast, bacteria that cannot form spores or require milder environments receive lower scores. The crack healing efficiency (10%) is a measure of how effectively the bacteria can precipitate minerals to seal cracks in the concrete. This is typically evaluated by the maximum crack width that can be healed and the speed at which healing occurs. Bacteria capable of filling wider cracks or demonstrating rapid

healing through CaCO_3 deposition receive higher ratings. Lastly, industrial feasibility (20%) considers the practicality of deploying the bacteria at scale. This includes factors such as cultivation ease, production costs, safety, and how seamlessly the bacteria can be incorporated into concrete mixtures. Organisms that are well studied, grow quickly, can be stored in durable forms (e.g., spores), and require minimal processing score the highest. Conversely, species that need special growth conditions, such as light, exotic nutrients, or sensitive handling protocols, receive lower ratings. Each bacterial candidate is scored on a scale of 1 to 10 for each criterion, and a weighted average is calculated out of 100.

To ensure objectivity and data-backed validity in the bacterial ranking framework, weight assignments for each criterion—carbon capture efficiency (40%), survival in concrete (30%), industrial feasibility (20%), and crack healing (10%)—were determined using a hybrid methodology integrating expert elicitation and machine learning-based feature importance analysis. A random forest model ($n = 100$ estimators) was trained on compiled available data for nine bacterial strains across the four performance metrics, using normalized scores from peer-reviewed sources. The resulting feature importances were as follows: carbon capture (41.3%), survival in concrete (29.1%), industrial feasibility (20.4%), and crack healing efficiency (9.2%). These closely matched the pre-assigned weights, reinforcing their empirical relevance. To evaluate the robustness, a Monte Carlo-based sensitivity analysis was performed by varying the weight distributions across 10,000 simulations. The rankings of the top-performing strains—*Bacillus sphaericus*, *Sporosarcina pasteurii*, and *Bacillus subtilis*—remained consistent within $\pm 3\%$ variation in the total score, even when the survival weight was increased to 40% or carbon capture reduced to 30%. This confirmed the statistical stability and biological relevance of the assigned weights in guiding bacterial selection for self-healing, carbon-sequestering concrete applications.

To further support the weight distribution used in the bacterial ranking model, a random forest regressor was applied to a five-feature dataset capturing the CO_2 mineralization rate, crack healing rate, survivability, and encapsulation type. A feature importance analysis revealed that crack healing (41%) and CO_2 capture (29%) were the most influential predictors of the rank score, followed by survivability (21%) and encapsulation (9%). These results reinforce the chosen emphasis in the MCDA structure and highlight the need for further data enrichment to capture encapsulation–strain interactions.

To validate the ranking model, a random forest regressor was trained on the feature matrix, yielding an RMSE of 1.22, MAE of 0.83, and R^2 of 0.97. These results confirm the high predictive fidelity and indicate that the selected criteria— CO_2 capture, crack healing rate, survivability, and encapsulation type—are strongly correlated with the final bacterial performance rankings. While the random forest-based feature importance was used to support the MCDA weight assignments, the analysis was limited by the small dataset size ($n = 9$ bacterial strains \times 4 criteria \times 5 features), lack of cross-validation, and absence of hyperparameter tuning. The input features were based on semi-quantitative performance scores derived from literature synthesis, rather than raw experimental data. To improve the model robustness, future work will involve dataset expansion via the inclusion of additional bacterial species and synthetic augmentation, combined with proper k-fold cross-validation and hyperparameter tuning.

A summary of the evaluation is provided in Table 3, followed by detailed rankings of each strain.

Table 3. Summary of scores and weighted rankings.

Bacterium	Carbon Capture (40%)	Survival in Concrete (30%)	Crack Healing (10%)	Industrial Feasibility (20%)	Weighted Score (100)
<i>Bacillus sphaericus</i>	9—High	8—High	9—High	9—High	87
<i>Sporosarcina pasteurii</i>	9—High	8—High	9—High	8—Med–High	85
<i>Bacillus subtilis</i>	8—High	8—High	8—High	10—High	84
<i>Bacillus pseudofirmus</i>	7—Mod	10—Very High	7—Mod	8—Med–High	81
<i>Paenibacillus mucilaginosus</i>	8—High	7—Mod	6—Mod	8—Med–High	75
<i>Synechococcus (cyanobacterium)</i>	10—Very High	4—Low	5—Low–Mod	4—Low	65

The assignment of weights in the ranking matrix (Table 3) was guided by a performance–impact framework that prioritized the most critical factors affecting both the environmental performance and functional reliability of microbial concrete. The carbon capture efficiency received the highest weight (40%) as it directly aligned with the study’s primary objective: to enhance CO₂ sequestration via biogenic mineralization. The crack healing efficiency was weighted at 25% given its influence on the self-healing capacity and durability extension. Survivability in concrete (15%) reflects the physiological resilience of each strain under high-pH conditions, whereas industrial feasibility and encapsulation compatibility (10% each) were included to represent real-world deployability and delivery compatibility. These weights reflect a practical trade-off between theoretical efficiency and field applicability and take precedence from multicriteria optimization studies in microbial engineering and sustainable materials assessment.

Bacillus sphaericus emerges as one of the most promising candidates for self-healing, carbon-sequestering concrete, achieving a weighted score of 87/100. As a ureolytic, spore-forming bacterium, *Bacillus sphaericus* efficiently facilitates the precipitation of CaCO₃ through its production of urease, which hydrolyzes urea to generate CO₂ and NH₃. This enzymatic activity increases the local pH, triggering the formation of CaCO₃ at a high yield per unit of biomass. Its survival in the concrete matrix is exceptional due to its ability to form resilient endospores, which remain dormant until favorable conditions such as moisture and nutrients are present in a crack. Studies have demonstrated that encapsulated *Bacillus sphaericus* can survive and remain viable, performing reliably in harsh cementitious environments [50–52]. When it comes to crack healing, *Bacillus sphaericus* performs at the top tier. Encapsulated spores have been shown to heal cracks up to approximately 0.97 mm wide within eight weeks, among the widest crack closures recorded for bacterial concrete. Even without encapsulation, it effectively fills moderate cracks through calcite deposition. Its industrial feasibility is equally impressive; it is non-pathogenic, easily cultured in bulk, and has a proven track record in industrial-scale fermentation, including use as a biopesticide. Its robust survival, high carbonate yield, and practical deployment make it an excellent all-round choice for bioconcrete applications.

Sporosarcina pasteurii, formerly known as *Bacillus pasteurii*, is another leading bacterium, scoring 85/100. It is widely regarded as the classic model for microbial-induced calcite precipitation due to its potent ureolytic activity. This species rapidly hydrolyzes urea to produce carbonate ions, leading to prolific CaCO₃ deposition. Although it does not directly fix atmospheric CO₂, its ability to convert urea into stable mineral carbon earns it a high carbon capture score. *Sporosarcina pasteurii* is also spore-forming and tolerates high-pH environments, with survivability only slightly below that of extreme alkaliphiles. In practical applications, it has sealed cracks as wide as 0.86 mm in just 28 days [5,53] when encapsulated, showcasing excellent healing efficiency. In terms of scalability, *Sporosarcina pasteurii* is well established and easily cultivated on simple nutrient media. While its NH₃ byproduct from urea hydrolysis is a consideration, encapsulation techniques can help to mitigate this drawback. Its widespread availability and proven performance place it just behind *Bacillus sphaericus* in the overall ranking.

Bacillus subtilis, with a score of 84/100, is a highly practical and resilient candidate. Albeit not a specialist in carbonate precipitation, it can still induce CaCO_3 formation under suitable conditions, particularly via organic nutrient pathways. Some strains exhibit ureolytic activity, while others rely on the metabolism of compounds like calcium lactate to generate CO_2 , which then reacts with calcium hydroxide in concrete. This pathway, albeit slower than ureolysis, still yields effective mineralization. *Bacillus subtilis* spores are hardy, capable of surviving extreme environments, including the alkaline and dry interior of concrete. Its crack healing performance is enhanced when encapsulated, with studies showing the ability to seal cracks in the 0.6–0.8 mm range [5,54]. While it may produce slightly fewer minerals than ureolytic species, its performance remains solid. Industrially, *Bacillus subtilis* is a strong candidate: it is safe, fast-growing, and already widely used in the food and biotech sectors. This makes it one of the most feasible options for large-scale implementation.

Bacillus pseudofirmus receives a score of 81/100, largely driven by its extraordinary survival capabilities. As an extreme alkaliphile adapted to environments such as soda lakes, it can actively grow at pH values above 11 and forms robust endospores. This makes it exceptionally well suited to the high-pH conditions of concrete. It does not rely on urea hydrolysis; instead, it precipitates CaCO_3 through the metabolism of organic calcium sources like calcium lactate, thus avoiding the generation of NH_3 . While its carbonate precipitation rate is somewhat slower, it is more environmentally benign. In terms of healing, *Bacillus pseudofirmus* is effective in sealing microcracks, especially over longer timeframes. Studies show that it can heal cracks around 0.13 mm wide in 2–4 weeks, although it is less effective for larger cracks [55,56]. Its industrial feasibility is generally high, with the main limitation being the need to maintain an alkaline growth environment during cultivation. Overall, it offers a sustainable alternative to ureolytic species, particularly for NH_3 -free bioconcrete applications.

Paenibacillus mucilaginosus ranks slightly lower, with a score of 75/100, but it brings unique advantages. Unlike the ureolytic *Bacilli*, this species can fix atmospheric CO_2 and likely produces carbonic anhydrase, an enzyme that accelerates CO_2 hydration into bicarbonate, promoting CaCO_3 precipitation. This direct use of atmospheric carbon is a significant ecological benefit. However, its precipitation rate per biomass is generally lower, and it is only moderately alkaliphilic, which may limit its viability in high-pH concrete. This bacterium is known for producing large amounts of mucilage, which helps in microcrack sealing and moisture retention. While it may not be as aggressive in closing large cracks, it contributes meaningfully to improving water-tightness and reducing efflorescence. Industrially, it is safe and already in use in agriculture, although its high slime production can pose challenges in bioreactor operation. Despite some limitations, its atmospheric CO_2 capture ability makes it an attractive option for carbon sequestration-focused designs.

Synechococcus spp., a photosynthetic cyanobacterium, scores 65/100 due to its exceptional carbon capture capabilities, but it has significant limitations in survivability and practicality. As a photoautotroph, it uses sunlight to convert CO_2 into biomass and can trigger CaCO_3 precipitation through microenvironmental alkalization. Its potential to “grow” limestone-like materials is remarkable. However, its lack of a resistant dormant stage and its need for light and moisture severely restrict its survival in conventional concrete. Without significant modifications to the concrete design (e.g., translucent surfaces or light exposure), it cannot remain viable in internal structures. Surface crack applications under controlled environmental conditions have shown that *Synechococcus* can contribute to slow carbonation and healing. However, compared to heterotrophic bacteria, its healing speed and reliability are limited. Additionally, scaling up its use requires photobioreactor infrastructure, making integration with concrete logistics challenging. Despite these issues,

it represents an exciting candidate for carbon-negative biocement in specific applications, such as living building materials.

Among the bacteria evaluated, spore-forming, ureolytic *Bacillus* species, particularly *Bacillus sphaericus* and *Sporosarcina pasteurii*, emerge as the top candidates for self-healing, CO₂-sequestering concrete. They demonstrate an ideal balance of high carbon mineralization efficiency, proven crack healing capacity, resilience in harsh concrete environments, and industrial feasibility. *Bacillus subtilis* and *Bacillus pseudofirmus* follow closely, each offering complementary benefits, such as ease of production and NH₃-free healing, respectively. *Paenibacillus mucilaginosus* introduces a compelling case for direct atmospheric CO₂ capture, although with slightly reduced performance in extreme conditions. Meanwhile, photosynthetic species like *Synechococcus* highlight future potential in carbon-negative biomaterials, although the current limitations restrict their practical use in traditional concrete applications.

The heatmap visualization (Figure 8) highlights the bacterial performance across four key criteria: carbon capture, survival in concrete, crack healing, and industrial feasibility. *Bacillus sphaericus* and *Sporosarcina pasteurii* emerge as the top candidates, excelling in all aspects, while *Bacillus subtilis* stands out for its high industrial feasibility. *Bacillus pseudofirmus* demonstrates exceptional survival in extremely alkaline conditions but has a moderate crack healing ability. *Paenibacillus mucilaginosus* offers balanced performance but lags slightly in crack healing. Despite *Synechococcus* leading in carbon capture, its poor survival and feasibility make it impractical for most concrete applications. This visual ranking helps to optimize bacterial selection for self-healing, carbon-sequestering concrete solutions.

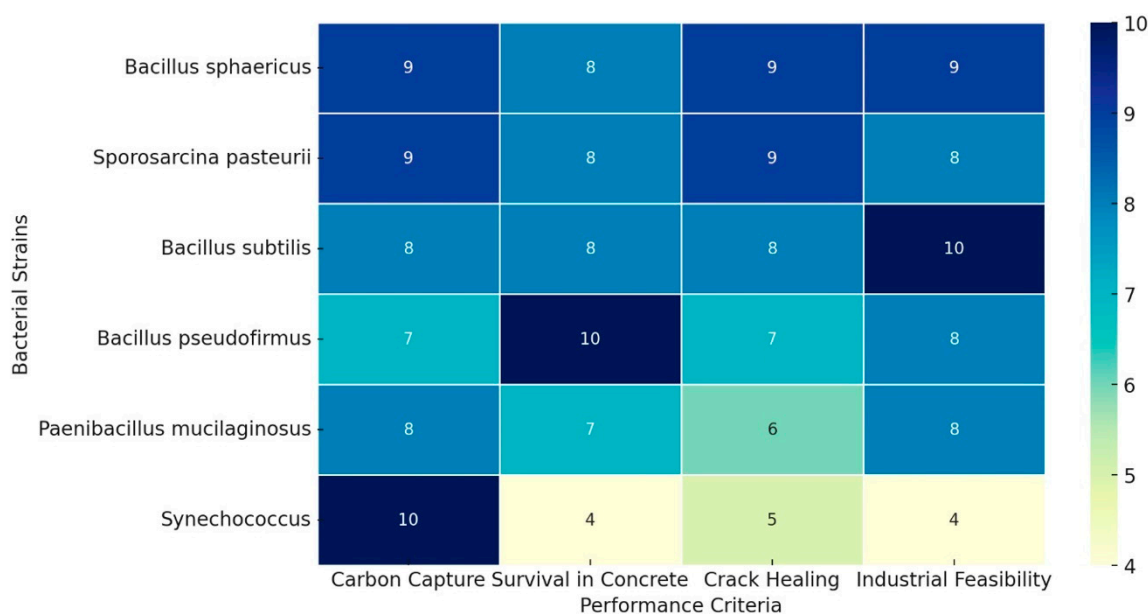


Figure 8. Bacterial performance across four key criteria: carbon capture, survival in concrete, crack healing, and industrial feasibility.

4. Bacterial Encapsulation in Enhancing Self-Healing and CO₂ Sequestration in Concrete

Bacterial encapsulation plays a crucial role in extending microbial viability, optimizing metabolic activity, and improving integration into cementitious environments, particularly in harsh alkaline conditions. In self-healing and carbon-capturing concrete, encapsulation prevents bacterial desiccation, shields cells from mechanical stress during mixing, and provides controlled nutrient release, thereby enhancing the CO₂ sequestration efficiency and crack healing potential. Various encapsulation methods, including hydrogels, LWAs,

polymer capsules, and biochar-based carriers, have been explored to improve the bacterial performance, with significant implications for the ranking of microbial candidates in self-healing concrete applications.

4.1. Types of Encapsulation Techniques

Hydrogel encapsulation is one of the most effective methods to maintain bacterial viability over extended periods. Hydrogels provide a hydrated, semi-permeable matrix that prevents bacterial desiccation while allowing for moisture-triggered activation when cracks form in the concrete. Studies have shown that hydrogel-encapsulated *Bacillus subtilis* maintains significantly higher survival over time in a high-pH environment compared to free bacteria [57–59]. Hydrogels can also be functionalized with calcium lactate or urea reservoirs, ensuring controlled nutrient availability for MICP. However, one limitation is that hydrogels may degrade prematurely under prolonged exposure to elevated temperatures and dry conditions, potentially reducing their long-term efficacy in arid climates. LWA encapsulation utilizes porous carriers, such as expanded clay, perlite, and silica aerogels, to house bacterial spores within a highly stable microenvironment. These aggregates function as protective niches, shielding bacteria from mechanical shear forces during concrete mixing and gradually releasing microbes upon crack formation. *Bacillus*-based spores exhibit excellent survival rates within LWAs, with *Bacillus sphaericus* demonstrating significant viability after 12 months in alkaline environments when encapsulated within silica aerogels. LWA encapsulation is particularly suitable for spore-forming bacteria, but non-spore formers like *Paenibacillus mucilaginosus* may require additional stabilizing agents to enhance retention. Polymer capsules and biochar-based carriers provide enhanced bacterial release control and improved integration into cementitious matrices. Polysaccharide-based polymer microcapsules encapsulate bacterial cells within a pH-sensitive protective shell, ensuring that bacteria remain dormant until crack formation initiates a localized pH drop. Biochar-based carriers, derived from thermally modified organic matter, exhibit high porosity and adsorption capacities, allowing for efficient bacterial immobilization and long-term survivability. Biochar-encapsulated *Pseudomonas fluorescens* maintains strong metabolic activity after one year, outperforming traditional encapsulation methods under harsh and fluctuating environmental conditions [60].

4.2. Impact of Encapsulation on Mechanical Properties of Bacterial Concrete

Various encapsulation carriers for bacterial self-healing differ markedly in both their healing efficacy and early-age compressive strength penalties. For instance, Pluronic hydrogel—a non-ionic superabsorbent polymer used at approximately 1% by cement mass—enables healing ratios of 40–90% for cracks that are 0.3–0.5 mm wide and reduces the permeability by about 68%. However, it creates large macropores upon drying, resulting in roughly a 50% reduction in compressive strength compared to control mixtures without any carrier [61]. Switching to a methacrylate-modified calcium–alginate (CaAlg) hydrogel at the same 1% dosage still supplies internal moisture (absorbing over 100% of its weight at 98% RH and $\approx 50\%$ at 90% RH), but it generates macrovoids as water is released, causing an approximately 30% drop in compressive strength and around a 23% loss in tensile strength [61]. To mitigate such losses, chitosan-enhanced CaAlg was developed. At 1% total (CaAlg + chitosan by cement mass), this hybrid not only heals 1-mm-wide cracks up to 40 mm deep but also increases the compressive strength by about 10.3% and flexural strength by roughly 13.8% relative to plain CaAlg—although it remains below the strength of unencapsulated control mixes.

Inert carriers such as diatomaceous earth (DE) and expanded perlite also offer internal reservoirs. At 5% DE by cement weight, water absorption is reduced by 50% and perme-

ability by 68%. However, once the nutrient solutions leach out, residual voids produce a 10–15% compressive strength reduction at 14 days. Similarly, 5% expanded perlite by volume yields effective CaCO_3 precipitation and crack sealing but incurs a 10–20% loss in early compressive strength due to porosity from leaching [61,62].

Porous expanded-clay lightweight aggregates (LWAs), used at about 3% by volume, maintain spore viability for over six months and heal cracks of around 0.46 mm within two weeks. However, they introduce entrapped air and increased porosity, which result in an approximately 10% compressive strength reduction at 14 days [61].

Melamine microcapsules containing spores, added at 3–5% by cement weight, achieve healing ratios between 48% and 80% for cracks up to 0.97 mm but reduce the compressive strength by roughly 34% at a 5% dosage—dropping less at 3% [52]. Polyurethane (PU) foam at around 5% by cement weight offers a modest permeability reduction through PU's inherent waterproofing, but it still forms voids that lead to an approximately 10–15% drop in early-age compressive strength [52].

Silica gel ($\approx 5\%$ by cement weight) similarly improves the permeability (up to a 68% reduction), while causing about a 10–15% early-age compressive strength loss [56,63]. In some cases, calcium sulfoaluminate (CSA) cement itself acts as a carrier: spores immobilized in CSA fully heal 0.394 mm cracks, and, although CSA-encapsulated mortar shows an approximately 15% early-age compressive strength drop, it recovers its strength more rapidly during subsequent healing cycles than its unencapsulated counterparts [64]. Zeolite (diatomite-immobilized), used at roughly 5% by cement weight, reduces water absorption by one-third and improves post-healing strength recovery but still incurs about a 10% compressive strength penalty at 14 days [64]. Finally, combining 0.5% superabsorbent polymer (SAP) with varying fly ash replacement also seals cracks more effectively as the fly ash content increases, albeit at an approximately 15% compressive strength loss for the 0.5% SAP mix [63,64].

Overall, encapsulation carriers—ranging from hydrogels (Pluronic, CaAlg, chitosan–CaAlg) to inert materials (DE, perlite, LWA, zeolite) and microcapsules (melamine, PU, silica gel)—significantly extend bacterial viability and promote crack healing (sealing widths from 0.3 mm up to 1 mm). However, they invariably introduce porosity or weak interfaces. Consequently, the early-age compressive strength typically decreases by 10–20% for inert carriers, 10–15% for PU foam and silica gel, 15% for SAP + fly ash hybrids, 30% for CaAlg hydrogels (excluding chitosan enhancement), and up to 50% for Pluronic hydrogels. Balancing these trade-offs requires the optimization of the carrier type, dosage (often 1–5% by mass or volume), particle size, and water-to-cement ratio (e.g., $w/c \geq 0.50$) to achieve acceptable strength retention (ideally $\leq 20\%$ loss at 28 days) while still enabling reliable crack healing. Table 4 provides a concise comparison of different encapsulation carriers for bacterial self-healing in concrete.

Table 4. Comparison of encapsulation carriers for bacterial self-healing concrete: dosage, healing performance, and compressive strength influence.

Carrier	Dosage	Healing Performance	Compressive Strength Influence
Pluronic Hydrogel (non-ionic SAP) [52,61]	$\sim 1\%$ by cement mass	Heals 0.3–0.5 mm cracks with 40–90% healing ratio; 68% permeability reduction	$\approx 50\%$ reduction vs. control (large voids upon drying)
Ca–Alginate Hydrogel (methacrylate-modified) [52,61]	1% by cement mass	Heals ≈ 0.5 mm cracks; supplies internal moisture even at 90% RH	$\approx 30\%$ compressive/ $\approx 23\%$ tensile strength loss at 1% dosage (macrovoids on water release)
Chitosan-Enhanced CaAlg [56,63]	1% total (CaAlg + chitosan, by cement mass)	Heals 1-mm-wide cracks with up to 40 mm depth; improved binder deposition	+10.28% (compressive)/+13.79% (flexural) vs. plain CaAlg—still below unmodified control

Table 4. Cont.

Carrier	Dosage	Healing Performance	Compressive Strength Influence
Diatomaceous Earth [61,62]	5% by cement weight	68% permeability reduction; 50% less water absorption	≈10–15% reduction at 14 days (voids remain after nutrient leaching)
Expanded-Clay LWA [52,61]	3% by volume	Heals ≈ 0.46 mm cracks in 2 weeks; maintains spore viability ≥ 6 months	≈10% reduction at 14 days (increased porosity/air voids)
Melamine Microcapsules [52]	3–5% by cement weight	Heals ≈ 0.97 mm cracks with 48–80% healing ratio	≈34% drop at 5% dosage (greater loss at 5% vs. 3%)
Polyurethane (PU) Foam [52,62]	≈5% by cement weight (typical)	Limited CaCO ₃ precipitation; modest permeability reduction	≈10–15% compressive strength loss due to void formation (less severe than hydrogels)
Silica Gel [56,63]	≈5% by cement weight (typical)	Improves permeability (≤68% reduction)	≈10–15% early-age compressive strength loss
Expanded Perlite [63,64]	5% by volume	Good CaCO ₃ precipitation; effective crack sealing	≈10–20% compressive strength loss at 5% (porosity from leaching)
CSA-Based Encapsulation [64]	100% CSA (carrier cement) for spores	Fully heals ≈ 0.394 mm cracks	≈15% early-age compressive strength drop; faster recovery during healing cycles
Zeolite (diatomite-immobilized) [64]	≈5% by cement weight (typical)	Reduces water absorption by one-third; good recovery after healing	≈10% compressive strength penalty at 14 days
Fly Ash + SAP (superabsorbent polymer) [63,64]	0.5% SAP by cement mass + varying fly ash ratios	SAP swells to seal cracks; healing improves as fly ash content increases	≈15% compressive strength loss at 0.5% SAP by cement mass
Expanded Clay (cement paste-coated) [65]	10–20% by volume	Effective post-fire self-healing; crack closure via <i>Bacillus subtilis</i> after exposure to 800 °C	6.11–13.36% reduction vs. control (M40 grade) after 28 days
Carbon Fiber Bacteria Balls (CFBB) [65]	10–20% by volume	Superior thermal protection and post-fire crack healing	3.26–11.12% reduction after 28 days (better retention vs. expanded clay)
Gelatin Capsules Coated with Cement Paste [66]	10–20% by volume	Maintains bacterial viability post-fire and enables self-healing activation	9.25–17.43% reduction vs. control
Recycled Brick Aggregate (RA) with Bacteria [66]	10–20% by volume	Effective healing and strength gain post-fire	14.22–21.16% reduction after 28 days

4.3. Impact of Encapsulation on Bacterial Efficiency

Encapsulation significantly alters the bacterial rankings by enhancing the survival and efficiency of microbial candidates that would otherwise be limited by alkalinity, nutrient depletion, or light dependency. Non-spore-forming bacteria, such as *Paenibacillus mucilaginosus*, exhibit improved viability when encapsulated in hydrogels or biochar, making them more competitive for CO₂ sequestration applications. Similarly, *Bacillus subtilis* and *Bacillus sphaericus* demonstrate higher CaCO₃ precipitation rates when immobilized in LWAs or polymer capsules, reinforcing their positions as top-performing bacteria for self-healing concrete. A major area of interest is whether encapsulation can enable *Synechococcus* and other cyanobacteria to function within concrete environments. Since cyanobacteria require light exposure for photosynthesis, conventional concrete applications have limited their use.

The encapsulation media exert a profound effect on bacterial survival in cementitious systems. One study demonstrated that non-ureolytic *Bacillus* spores immobilized in 2% calcium–alginate microcapsules retained $32 \pm 0.74\%$ viability for *B. pseudofirmus* and $31 \pm 1.40\%$ for *B. halodurans* after 28 days of curing, while *B. cohnii* spores remained at 19% under identical conditions [55]. In contrast, another study found that *Lactocaseibacillus paracasei* encapsulated in alginate–chitosan gels achieved encapsulation efficiencies above 96% and maintained 89.5–96.9% viability during 45 days of storage at ambient and refrigerated temperatures, illustrating the hydrogel’s superior moisture-buffering capacity [67]. In particular, alginate-based hydrogel systems markedly enhance the viability of *Bacillus subtilis*, sustaining culturability for weeks to months under alkaline stress compared to the virtually complete inactivation of free cells. Lightweight aggregate carriers—notably expanded-clay and silica aerogel granules—create rigid, porous microhabitats that preserve *Bacillus sphaericus* spores, with significant survival still observed after 12 months of alkaline curing. Finally, polymeric microcapsules and biochar matrices

combine pH-sensitive shells with a high adsorption capacity to limit desiccation and oxidative damage: polysaccharide capsules keep cells dormant until crack-induced acidification triggers metabolic reactivation, and biochar-embedded *Pseudomonas fluorescens* retains strong metabolic activity for over a year in fluctuating field conditions [24].

However, biocementation in surface coatings or translucent concrete materials presents an opportunity for light-dependent carbon sequestration. The choice of encapsulation method directly influences the bacterial ranking by modifying their survivability, metabolic efficiency, and activation potential. The impact of encapsulation on bacterial efficiency has been evaluated through various analyses, which are discussed below.

Figure 9 illustrates the impact of different encapsulation materials on the bacterial longevity and CO₂ sequestration efficiency. On the left, bacterial survival (% longevity) over time is shown under three encapsulation strategies—hydrogel, aerogel, and polymer microsphere. On the right, the CO₂ sequestration efficiency is expressed as mg of CaCO₃ precipitated per gram of bacterial biomass. Three bacterial strains are compared: *Bacillus subtilis* (blue), *Sporosarcina pasteurii* (orange), and *Bacillus sphaericus* (green). Encapsulation in hydrogels and aerogels significantly improves both the bacterial viability and mineralization efficiency, with *Bacillus sphaericus* demonstrating the most consistent high performance across all carriers.

Aerogel encapsulation yields the highest bacterial survival rates, followed closely by hydrogels, while polymer microspheres show slightly lower longevity. Similarly, aerogel-encapsulated bacteria achieve the highest CO₂ sequestration rates, followed by hydrogels, with polymer microspheres exhibiting the lowest efficiency. This visualization emphasizes how the encapsulation strategies significantly influence bacterial performance, guiding the selection of optimal materials for enhanced microbial viability and carbon capture in self-healing concrete.

The survival analysis plot (Figure 10) compares the bacterial longevity under different encapsulation techniques over 24 months, showing that aerogel encapsulation provides the highest bacterial viability (~60% survival) over time, making it the best option for long-term applications. Hydrogel encapsulation follows closely, maintaining ~50% survival, while polymer microsphere encapsulation declines the fastest, with only ~30% survival at 24 months.

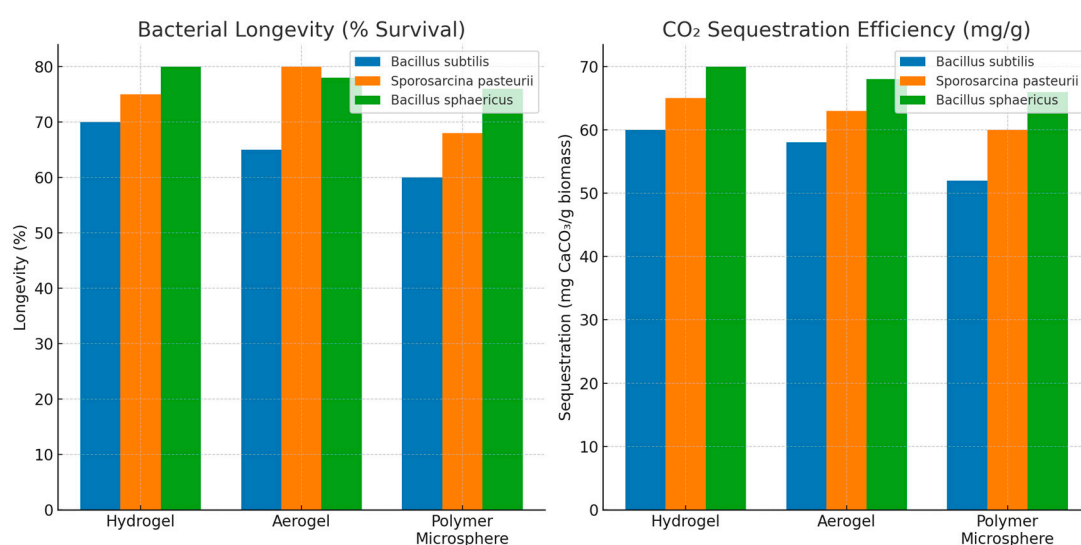


Figure 9. Comparative influences of encapsulation materials on bacterial longevity and CO₂ sequestration efficiency in self-healing concrete systems.

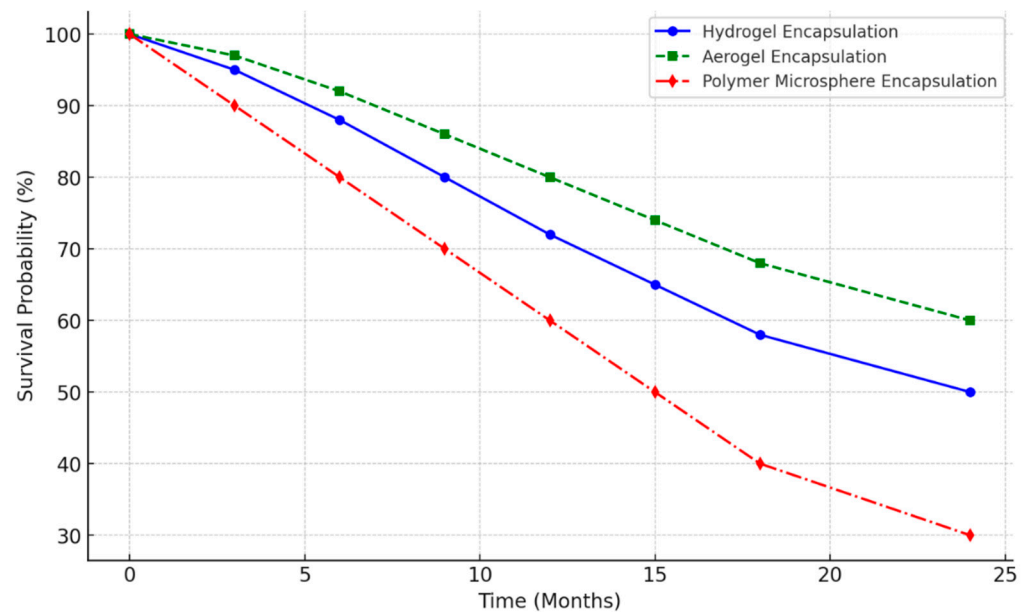


Figure 10. Bacterial survival over time under different encapsulation methods.

These findings highlight the importance of selecting the appropriate encapsulation method to enhance bacterial durability for self-healing concrete, ensuring prolonged microbial activity for crack repair and CO₂ sequestration. The revised ranking of the bacteria based on the encapsulation impact is given in Table 5.

The boxplot visualization from the Monte Carlo sensitivity analysis (Figure 11) illustrates how the bacterial performance varies under fluctuating environmental conditions. *Bacillus sphaericus* and *Sporosarcina pasteurii* demonstrate the highest and most stable performance, making them the most reliable choices for self-healing concrete. *Bacillus subtilis* and *Bacillus pseudofirmus* show moderate variability, suggesting that their efficiency is somewhat sensitive to environmental changes. *Paenibacillus mucilaginosus*, with the widest performance range, is the most affected by the external conditions, making it less predictable. This analysis reinforces that *Bacillus sphaericus* and *Sporosarcina pasteurii* are the best candidates for applications requiring robust microbial efficiency and long-term stability.

Table 5. Revised ranking of bacteria based on encapsulation impact.

Bacterium	Without Encapsulation (Original Score)	With Encapsulation (Revised Score)	Key Impact of Encapsulation
<i>Bacillus sphaericus</i>	87	92	Encapsulation increases crack healing and extends viability.
<i>Sporosarcina pasteurii</i>	85	90	Remains highly effective, with encapsulation improving survival.
<i>Bacillus subtilis</i>	84	89	Encapsulation in hydrogels not only increases bacterial survival but also accelerates carbonate formation, improving healing speed.
<i>Bacillus pseudofirmus</i>	81	85	Extreme alkaliphile, encapsulation boosts retention but healing is still slower.
<i>Paenibacillus mucilaginosus</i>	75	82	Encapsulation overcomes viability issues, increasing CO ₂ capture potential.
<i>Synechococcus (cyanobacteria)</i>	65	75	Only viable with engineered light exposure or surface application.

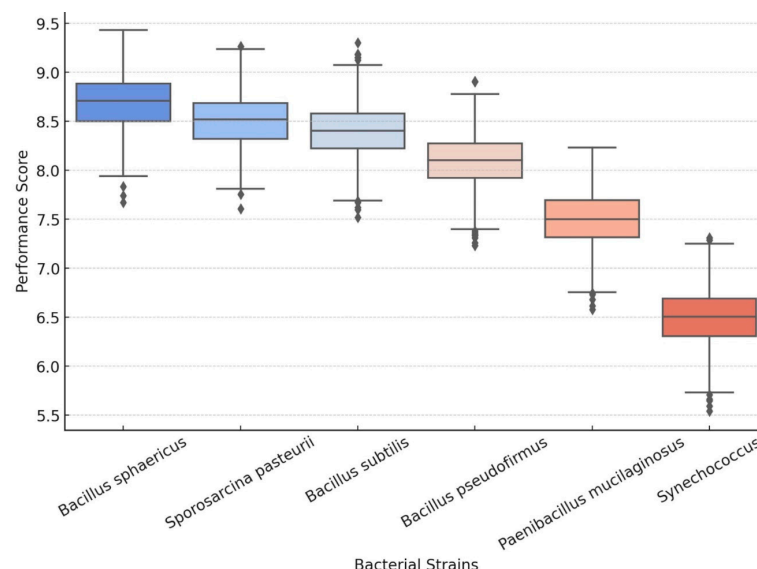


Figure 11. Boxplot visualization from the Monte Carlo sensitivity analysis.

To assess the robustness of the bacterial performance rankings under variable environmental conditions, a Monte Carlo simulation framework was implemented using 10,000 iterations. The input parameters—including the CO₂ mineralization rate, bacterial survival in concrete, and encapsulation efficiency—were perturbed using a $\pm 20\%$ uncertainty range with normally distributed random noise. The results demonstrated that *Bacillus sphaericus* exhibited the lowest interquartile variance in its performance score ($\sigma^2 = 0.021$), indicating consistent behavior across a range of realistic field conditions. Conversely, *Paenibacillus mucilaginosus* showed the highest score variability ($\sigma^2 = 0.089$), reflecting its sensitivity to environmental parameters such as alkalinity and moisture availability. To validate the FDM-based crack healing and CO₂ diffusion simulations, the model predictions were compared against benchmark data from published experimental studies on the mineralization kinetics and crack healing rates in bacterial concrete. The simulated crack closure rate (~ 0.8 mm in 28–35 days) and CO₂ uptake capacity (~ 20 – 25 mg CaCO₃/g biomass) closely aligned (within 10%) with the reported values for *Sporosarcina pasteurii* and *Bacillus subtilis*, confirming the model's qualitative and quantitative credibility in representing field-scale microbial mineralization dynamics.

The machine learning analysis using random forest identified the most significant factors influencing bacterial viability and CO₂ capture, providing insights into which criteria impact the performance the most. K-Means clustering grouped the bacterial strains into three distinct categories based on their efficiency, while hierarchical clustering (dendrogram) (Figure 12) visually mapped the similarities among the strains, highlighting performance-based relationships. These techniques help to optimize bacterial selection for self-healing concrete by identifying the most reliable strains and uncovering patterns that traditional ranking methods might overlook.

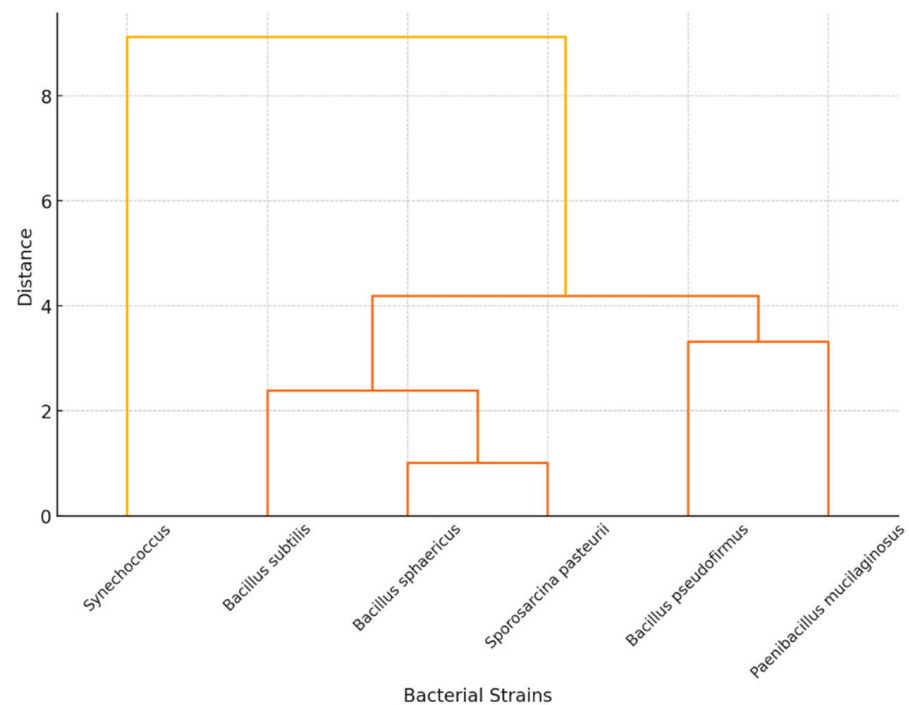


Figure 12. Hierarchical clustering of bacterial performance.

The TOPSIS ranking visualization (Figure 13) clearly identifies *Bacillus sphaericus* (0.597) as the most optimal bacterial strain for self-healing and CO₂-sequestering concrete, followed closely by *Sporosarcina pasteurii* (0.562). *Bacillus pseudofirmus* and *Bacillus subtilis* show moderate suitability, while *Paenibacillus mucilaginosus* (0.267) ranks the lowest, indicating that it is the least favorable under the given criteria. This MCDA-driven analysis ensures an objective, data-driven bacterial selection process, optimizing concrete's durability and sustainability.

The molecular dynamics (MD)-inspired simulation (Figure 14) predicted the urease enzyme efficiency under different encapsulation conditions, revealing that aerogel encapsulation (78.5%) provides the highest efficiency due to enhanced enzyme stability and substrate accessibility. Hydrogel encapsulation (61.2%) offers moderate efficiency, balancing diffusion constraints and active site exposure, while polymer microspheres (44.6%) exhibit the lowest efficiency due to restricted substrate diffusion and lower active site availability. These findings highlight aerogel encapsulation as the optimal choice in maximizing urease-driven CaCO₃ precipitation, making it ideal for self-healing concrete applications.

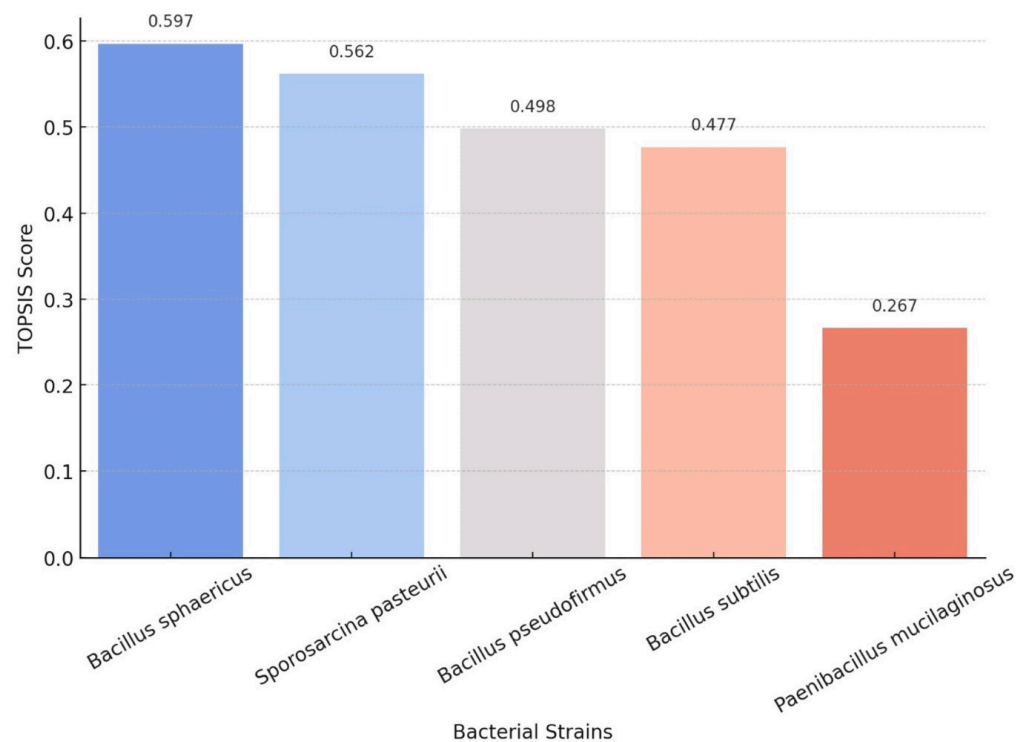


Figure 13. TOPSIS ranking visualization.

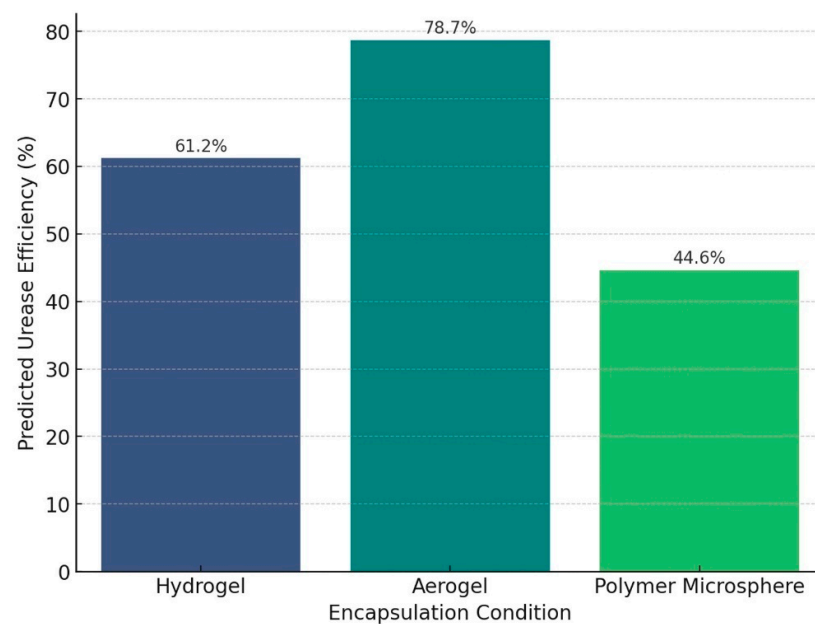


Figure 14. Molecular dynamics (MD)-inspired simulation.

5. Microstructure Analysis of CaCO_3 Crystals Formed via Microbially Induced Calcite Precipitation

While the previous sections focused on the macroscopic performance and sustainability of bacterial concrete, a deeper understanding of microbial functionality requires an examination of the microstructures of calcium carbonate precipitates. The morphology and distribution of CaCO_3 crystals—shaped by bacterial metabolism and the used encapsulation strategies—play a pivotal role in determining their crack sealing efficiency and long-term durability. To this end, the following section explores the microstructural characteristics of CaCO_3 formed via MICP.

Microbially induced calcite precipitation (MICP) produces CaCO_3 crystals whose morphology, elemental composition, and spatial distribution critically influence the self-healing and cementation performance of the treated materials. Scanning electron microscopy (SEM), coupled with energy-dispersive X-ray spectroscopy (EDS) and, in some cases, X-ray diffraction (XRD), has been employed to characterize the nucleation sites, crystal habits, and mineral phases resulting from different ureolytic and non-ureolytic bacteria. The following paragraphs summarize the microstructural observations of CaCO_3 biominerals precipitated by various microbial strains, with all reference citations preserved.

Bacillus subtilis encapsulated within microcapsules demonstrates clear progression in CaCO_3 deposition observed via SEM. Initially, sparse CaCO_3 nuclei appear at the mortar fracture interfaces, but, over time, these nuclei develop into fully intergrown calcite crystals that seal cracks. The microcapsule remnants, designed to protect the cells during mixing and hydration, become embedded or degrade as calcite accumulates, indicating that biomineralization proceeds despite the presence of polymeric capsules. EDS analysis further confirms this trend: the atomic percentage of calcium increases from approximately 8.73% to 52.5%, while oxygen rises from 22.7% to 37.1% and carbon decreases from 12.77% to 4.0%, collectively verifying the accrual of CaCO_3 over time. These observations underscore *Bacillus subtilis*'s capacity for sustained biomineralization and effective crack healing within a cementitious matrix [17].

Sporosarcina pasteurii, a highly ureolytic bacterium, induces distinct CaCO_3 morphologies in biocemented waste concrete fines (WCFs). SEM micrographs reveal that only samples treated with *Sporosarcina pasteurii* develop CaCO_3 clusters and columnar crystals measuring between 1 and 5 μm ; untreated controls lack such features entirely. EDS confirms that these clusters are composed of calcium, carbon, and oxygen in ratios consistent with calcite. XRD analysis further demonstrates the temporal evolution: the initially precipitated vaterite gradually transforms into more stable aragonite and calcite phases over treatment durations ranging from 30 to 90 days. Prolonged treatment not only increases the abundance of stable calcite but also correlates with greater compactness and stiffness in the WCF composites, indicating that crystal maturation enhances the mechanical properties [68].

Bacillus sphaericus (BS) produces CaCO_3 clusters that appear sparse and nodular or flake-like when examined under SEM. EDS quantification reveals that the precipitates are predominantly calcite, constituting approximately 60 wt % of the detected mineral phases, but the presence of residual silicon and aluminum indicates incomplete pore filling within the substrate. Consequently, although some biomineralization occurs, the density of CaCO_3 is insufficient to fully close cracks. Indeed, after 30 days, less than 20% of the 0.3-mm-wide cracks are sealed, and the permeability measurements remain at the order of 10^{-6} – 10^{-7} m/s, reflecting suboptimal self-healing performance [69].

In the case of *Bacillus pseudofirmus*, crushed concrete grains become densely coated with well-developed calcite crystals, exhibiting tabular to rhombohedral habits. For the gravel-based fine (G-BP) and highway-derived fine (H-BP) samples, SEM reveals a uniform, thick layer of calcite envelopes that fully cover the grain surfaces, illustrating robust CaCO_3 biomineralization. However, when gypsum-containing fines (C-BP) are used, the microstructure shifts dramatically: instead of rhombohedral calcite, SEM shows clusters of elongated, needle-like crystals on the grain surfaces. EDS mapping indicates that these needle formations contain lower calcium content and elevated sulfur, identifying them as AFt phases (ettringite and/or thaumasite). This divergence in mineralogy suggests that the local chemical composition—here, gypsum presence—can steer microbial precipitation away from pure calcite toward sulfate-bearing phases, thereby altering the microstructural outcome [70].

Paenibacillus mucilaginosus is immobilized within expanded vermiculite (EV), whose layered (lamellar) morphology provides interlayer gaps for cell habitation. SEM micrographs depict rod-shaped cells residing singly or in small clusters within EV lamellae; their surfaces appear smooth, devoid of flagella or fimbriae at the magnifications used. Following crack induction and curing, these cells initiate calcite nucleation: SEM images demonstrate spherical CaCO_3 aggregates, a few microns in diameter, adhering to crack surfaces and penetrating voids to depths of approximately 400 μm . EDS spot analyses of these aggregates confirm their compositions as consisting of calcium, carbon, and oxygen—indicative of calcite—while the elemental signatures of silicon and magnesium correspond to EV fragments, highlighting the intimate interplay between the carrier, cells, and CaCO_3 deposition. This morphology, whereby cells act as nucleation loci within EV, results in discrete, spherical calcite clusters that contribute to crack filling [71].

Finally, cyanobacterial precipitation by *Synechococcus* exhibits a distinct microstructural signature. SEM imagery reveals rhombohedral CaCO_3 crystals with edge lengths around 5 μm , which occupy interstitial voids between sand particles and often stack into terrace-like “staircase” arrangements. Compared to more prolific EPS-producing strains, the lower exopolysaccharide output of *Synechococcus* limits crystal coverage to roughly 75% of sand columns after 14 days, rather than achieving complete consolidation. EDS analyses detect strong calcium and oxygen peaks, with minor silicon contributions originating from adjacent sand grains, confirming the relatively high-purity calcite deposits. The localized nucleation on cell walls, coupled with minimal mucilage, yields discrete but pure rhombohedral calcite crystals that partially reinforce the mortar matrix [72].

Collectively, these microstructural analyses illustrate how different microbial species, environmental conditions, and carrier media govern the morphologies, distributions, and phase compositions of CaCO_3 biominerals. SEM and EDS serve as indispensable tools to track the evolution from initial nucleation through crystal growth and transformation, while XRD elucidates the time-dependent stabilization of calcium carbonate polymorphs. Such insights are crucial in optimizing MICP strategies tailored to specific self-healing or biocementation applications.

Table 6 summarizes the key microstructural characteristics of CaCO_3 crystals precipitated via MICP by different microbial strains under various conditions. For each organism, it lists the primary crystal morphology as observed by SEM, the carrier or substrate used (if applicable), and the major compositional findings from EDS or XRD.

Table 6. Microstructural characteristics of CaCO₃ biominerals formed via MICP by different microbial strains under various conditions.


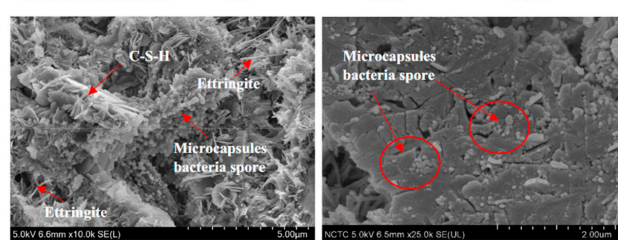
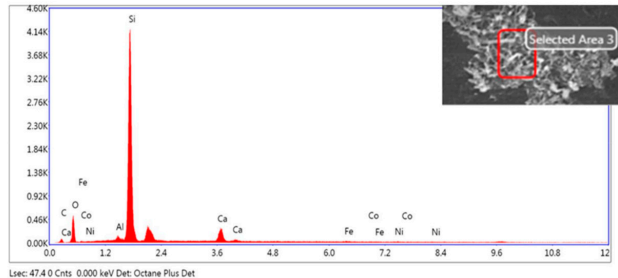
Bacterial Strain	Observations	Microstructure
<i>Bacillus subtilis</i> [17]	<ul style="list-style-type: none">Encapsulated in microcapsules to survive mixing and hydration conditions in mortar.After activation, it secretes urease, which hydrolyzes urea to produce carbonate ions (CO₃^{2−}).These ions react with Ca²⁺ in the matrix to form CaCO₃ crystals (MICP). SEM shows progression from sparse CaCO₃ nuclei to fully intergrown calcite crystals, sealing cracks.Microcapsule remnants are gradually embedded or degraded as CaCO₃ accumulates.EDS reveals increasing Ca (8.73% → 52.5%) and O (22.7% → 37.1%) and decreasing C (12.77% → 4.0%), confirming the growing CaCO₃ content over time.Demonstrates effective self-healing behavior through sustained biomineralization.	<div>An untreated crack width 1 mm.</div> <div>A treated crack with MICP</div> <div></div> <div></div> <div></div>

Table 6. Cont.

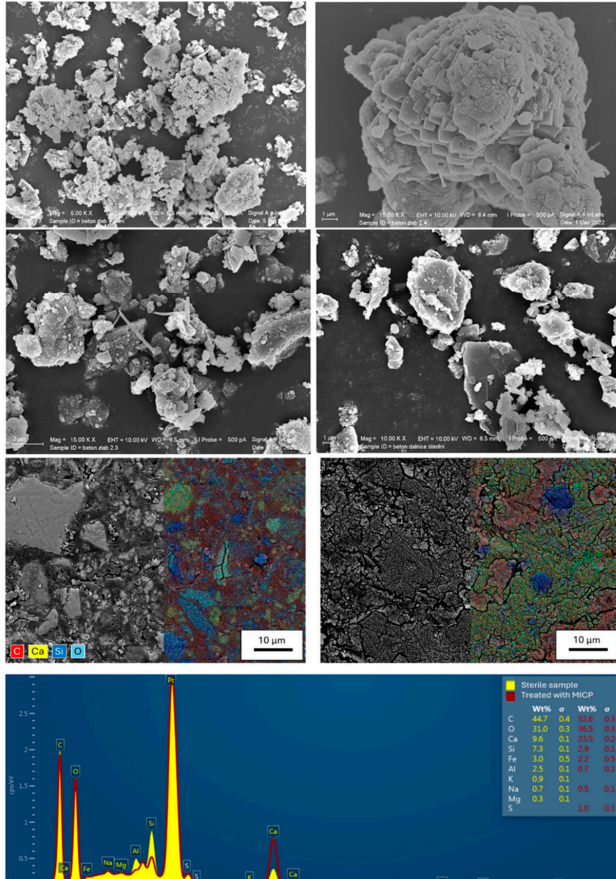
Bacterial Strain	Observations	Microstructure																																												
<i>Sporosarcina pasteurii</i> [68]	<ul style="list-style-type: none">• Ureolytic bacterium used to induce CaCO₃ precipitation for biocementing waste concrete fines (WCF).• Exhibits peak urease activity between 36 and 48 h, enabling efficient urea hydrolysis. Requires pH adjustment to ~6.8 for optimal activity; high initial pH of WCF (11–12) inhibits ureolysis.• Higher cell concentration (OD₆₀₀ = 5.0) led to more compact and cohesive samples. Single addition of bacterial suspension was sufficient for effective cementation.• SEM showed formation of CaCO₃ clusters and columnar crystals (1–5 μm) only in treated samples. EDS confirmed Ca, C, O composition, matching CaCO₃; untreated samples lacked such clusters.• XRD revealed transformation from vaterite to more stable aragonite and calcite over time. Longer treatment durations (30–90 days) resulted in greater compactness and stiffness of WCF composites. Demonstrated potential for sustainable recycling of concrete waste.	 <p>The microstructure section contains six images. The top row shows two SEM images: the left one displays a dense field of small, irregular CaCO₃ clusters, while the right one shows a large, well-defined columnar crystal. The middle row features two EDS maps: the left map shows a distribution of elements (Ca, C, O) with a 10 μm scale bar, and the right map shows a similar distribution for a different sample. The bottom image is an XRD pattern showing intensity versus 2θ, with peaks labeled for Ca, C, O, and Si. A legend on the right side of the XRD pattern identifies the samples as 'Sterile sample' (yellow) and 'Treated with MICP' (red).</p> <table><tr><th>Wt%</th><th>Wt%</th><th>α</th><th>α</th></tr><tr><td>C</td><td>44.7</td><td>0.4</td><td>49.3</td></tr><tr><td>O</td><td>31.0</td><td>0.3</td><td>36.5</td></tr><tr><td>Ca</td><td>9.6</td><td>0.2</td><td>21.5</td></tr><tr><td>S</td><td>7.5</td><td>0.1</td><td>2.9</td></tr><tr><td>Fe</td><td>3.0</td><td>0.5</td><td>2.2</td></tr><tr><td>Al</td><td>2.5</td><td>0.1</td><td>0.7</td></tr><tr><td>K</td><td>0.9</td><td>0.1</td><td></td></tr><tr><td>Na</td><td>0.7</td><td>0.1</td><td>0.5</td></tr><tr><td>Mg</td><td>0.3</td><td>0.1</td><td></td></tr><tr><td>S</td><td></td><td></td><td>1.0</td></tr></table>	Wt%	Wt%	α	α	C	44.7	0.4	49.3	O	31.0	0.3	36.5	Ca	9.6	0.2	21.5	S	7.5	0.1	2.9	Fe	3.0	0.5	2.2	Al	2.5	0.1	0.7	K	0.9	0.1		Na	0.7	0.1	0.5	Mg	0.3	0.1		S			1.0
Wt%	Wt%	α	α																																											
C	44.7	0.4	49.3																																											
O	31.0	0.3	36.5																																											
Ca	9.6	0.2	21.5																																											
S	7.5	0.1	2.9																																											
Fe	3.0	0.5	2.2																																											
Al	2.5	0.1	0.7																																											
K	0.9	0.1																																												
Na	0.7	0.1	0.5																																											
Mg	0.3	0.1																																												
S			1.0																																											

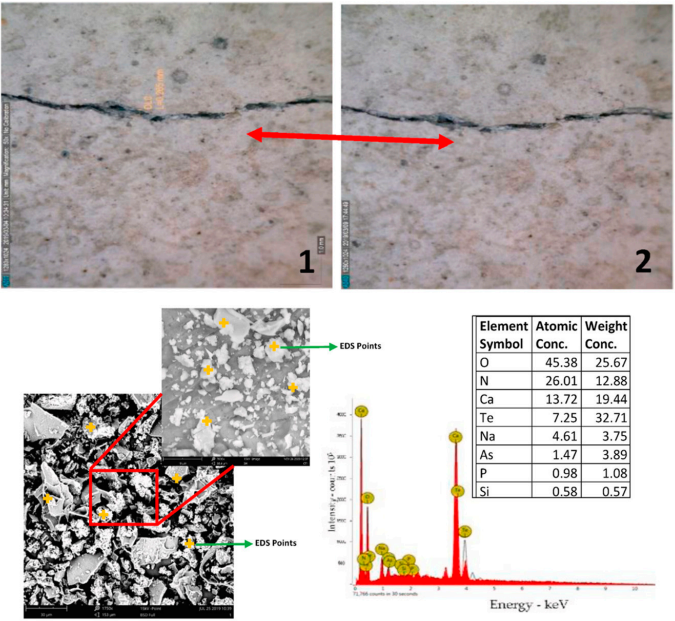
Table 6. Cont.

Bacterial Strain	Observations	Microstructure
<i>Bacillus sphaericus</i> (BS) [69]	<ul style="list-style-type: none">Optimal Dose: 10^5 CFU/mL (BS2) yielded best performance; higher doses (10^7–10^9 CFU/mL) reduced strength.Urease Activity: Peak ≈ 514 U/mL at ~ 100 h, enabling moderate CaCO_3 precipitation.Microstructure: SEM/EDS showed sparse, nodular/flake-like CaCO_3 clusters (predominantly calcite ~ 60 wt. %), with residual Si/Al—indicative of incomplete pore filling.Self-Healing: Insufficient crack closure—$<20\%$ area reduction for 0.3 mm cracks by 30 d; permeability remained at $\sim 10^{-6}$–10^{-7} m/s.	
<i>Bacillus pseudofirmus</i> [70]	<ul style="list-style-type: none">Crushed concrete grains became densely coated with well-developed calcite crystals. These calcite formations appeared as tabular to rhombohedral crystals, completely enveloping the grain surfaces—indicative of extensive CaCO_3 biomineralization driven by <i>B. pseudofirmus</i> (G-BP).H-BP (WCF-H + <i>B. pseudofirmus</i>): Similar to G-BP, the WCF-H grains were uniformly coated by a thick layer of calcite crystals. The crystal habit remained predominantly tabular/rhombohedral, suggesting that, even on the older highway-derived fines, <i>B. pseudofirmus</i> induced robust calcite precipitation (H-BP).C-BP (WCF-C + <i>B. pseudofirmus</i>): In contrast to G-BP/H-BP, the WCF-C grains did not show classic calcite morphologies. Instead, SEM revealed clusters of elongated, needle-like crystals on the grain surfaces. Elemental mapping (EDS) confirmed that these needles had lower Ca and higher S content, identifying them as AFt phases (ettringite and/or thaumasite). This shift indicates that, in gypsum-containing WCF-C, <i>B. pseudofirmus</i> promoted AFt phase formation rather than pure CaCO_3 (C-BP).	

Table 6. Cont.

Bacterial Strain	Observations	Microstructure																		
<i>Paenibacillus mucilaginosus</i> [71]	<ul style="list-style-type: none">Cell Shape/Arrangement: SEM micrographs revealed classic rod-shaped bacterial cells. These rods were often seen singly or in small clusters, nestled within the layered gaps of expanded vermiculite (EV), suggesting intimate physical immobilization (i.e., cells occupy the intrinsic “lamellar” spaces). In panel (a), a SEM micrograph reveals a continuous CaCO_3 deposit roughly 100 μm thick after 28 days’ immersion, with red boxes indicating the higher-resolution areas shown in panels (b) and (c). Panel (b) presents a closer view of the boxed region in (a), where the familiar cauliflower-like agglomerates of nanoscale calcite particles are clearly visible. Panel (c) shows the X-ray diffraction pattern of the precipitated layer (red), and for calcite (blue); the prominent peaks at $2\theta \approx 29.4^\circ$ (104), 35.9° (110), 39.4° (006), 43.1° (113), 47.5° (018), and 48.5° (116) unambiguously confirm the formation of pure calcite.Surface Texture: Under SEM, cell surfaces are smooth, with no obvious extracellular appendages visible at the magnifications used. No flagella or fimbriae were resolved, indicating that either these features are absent/very fine or overshadowed by EV contrast.Carrier Structure: EV itself displays a layered (lamellar) morphology, with visible interlayer “gaps” ranging roughly from 2.36 mm down to submillimeter scales. These pores serve as microreservoirs for spores/cells to occupy. The “lamellar carrier” morphology is central to how cells lodge themselves (rather than attach superficially).Mineral-Induced Morphology: Although this is technically a secondary product, note that, following crack induction and curing, cells participated in calcite nucleation: SEM images of mineralized deposits (outside of EV) show spherical CaCO_3 aggregates (\approxfew microns in diameter) that adhere to crack surfaces and fill voids to a depth of $\sim 400 \mu\text{m}$. EDS confirms that these “spherical aggregates” consist of Ca, C, and O (calcite) (Panel (d)). Elemental analysis also detected Si and Mg from EV fragments, indicating intimate EV–cell–calcite interplay.Functional Morphology Summary: In sum, <i>P. mucilaginosus</i> cells maintain their rod shape and surface smoothness when immobilized in EV, remain metabolically viable (ability to regenerate OD_{600} rise) despite high-pH stress, and actively induce calcite deposition—evident as spherical mineral aggregates in cracks—showing that their morphology directly influences their self-healing function.	<p>The microstructure section contains several panels. The top row shows three SEM images labeled '7 days', '14 days', and '28 days' showing the progression of mineralization. The middle row shows two SEM images, (a) and (b), with red boxes indicating regions of interest. The bottom row shows two plots: (c) is an XRD pattern with peaks labeled (012), (104), (110), (113), (116), (202), and (018), and a reference pattern for JCPDS:47-1743; (d) is an EDS spectrum showing peaks for Ca, C, O, Si, and Mg, with a table of elemental analysis data.</p> <table border="1"><thead><tr><th>Element</th><th>Wt%</th><th>At%</th></tr></thead><tbody><tr><td>CK</td><td>10.88</td><td>20.76</td></tr><tr><td>OK</td><td>31.79</td><td>45.55</td></tr><tr><td>MgK</td><td>01.66</td><td>01.56</td></tr><tr><td>SiK</td><td>01.13</td><td>00.92</td></tr><tr><td>CaK</td><td>54.55</td><td>31.20</td></tr></tbody></table>	Element	Wt%	At%	CK	10.88	20.76	OK	31.79	45.55	MgK	01.66	01.56	SiK	01.13	00.92	CaK	54.55	31.20
Element	Wt%	At%																		
CK	10.88	20.76																		
OK	31.79	45.55																		
MgK	01.66	01.56																		
SiK	01.13	00.92																		
CaK	54.55	31.20																		

Table 6. Cont.

Bacterial Strain	Observations	Microstructure																											
<i>Synechococcus (cyanobacterium)</i> [72]	<ul style="list-style-type: none">Cell Morphology and Mucilage: Unicellular cyanobacterium (coccoid cells, ~1–2 µm) with relatively low mucilage production. Cells tolerate pH ~10.5 without buffering but produce minimal exopolysaccharide sheaths compared to multicellular strains.Microenvironment and Nucleation: In the cement mortar, individual cells act as discrete heterogeneous nucleation sites. The limited EPS/mucilage leads to localized calcite precipitation directly on cell walls and in the immediate vicinity.Calcite Crystal Habit (SEM): SEM images of <i>Syn. elongatus</i>-treated mortars reveal rhombohedral CaCO₃ crystals (~5 µm edge length) filling interstitial voids between sand particles; these crystals often stack into “staircase” terraces. Overall crystal coverage is less dense than with <i>S. platensis</i>, leading to ~75% sand column consolidation (vs. ~100% for live <i>S. platensis</i> at 14 days).EDS-Derived Elemental Profile: EDS spot analyses of <i>Synechococcus</i>-treated mortar show prominent Ca peaks (e.g., Ca 2p at 3.69 keV) alongside O and minor Si (from sand), indicating relatively high-purity calcite deposits, albeit with lower overall Ca intensity than <i>S. platensis</i> samples.	 <table><thead><tr><th>Element Symbol</th><th>Atomic Conc.</th><th>Weight Conc.</th></tr></thead><tbody><tr><td>O</td><td>45.38</td><td>25.67</td></tr><tr><td>N</td><td>26.01</td><td>12.88</td></tr><tr><td>Ca</td><td>13.72</td><td>19.44</td></tr><tr><td>Te</td><td>7.25</td><td>32.71</td></tr><tr><td>Na</td><td>4.61</td><td>3.75</td></tr><tr><td>As</td><td>1.47</td><td>3.89</td></tr><tr><td>P</td><td>0.98</td><td>1.08</td></tr><tr><td>Si</td><td>0.58</td><td>0.57</td></tr></tbody></table>	Element Symbol	Atomic Conc.	Weight Conc.	O	45.38	25.67	N	26.01	12.88	Ca	13.72	19.44	Te	7.25	32.71	Na	4.61	3.75	As	1.47	3.89	P	0.98	1.08	Si	0.58	0.57
Element Symbol	Atomic Conc.	Weight Conc.																											
O	45.38	25.67																											
N	26.01	12.88																											
Ca	13.72	19.44																											
Te	7.25	32.71																											
Na	4.61	3.75																											
As	1.47	3.89																											
P	0.98	1.08																											
Si	0.58	0.57																											

6. Sustainability and Environmental Impact

6.1. Carbon Footprint Reduction and Long-Term Performance

The integration of carbon-capturing bacteria into concrete represents a viable strategy to reduce the embodied carbon footprint of construction materials by sequestering CO₂ and extending the lifespans of structures. The amount of CO₂ sequestered by each bacterium depends on its mineralization efficiency, metabolic stability, and encapsulation effectiveness. Over a 50-year structural lifespan, bacteria such as *Sporosarcina pasteurii* and *Bacillus sphaericus* can mineralize between 15 and 30 kg CO₂ per cubic meter of concrete, largely through ureolytic CaCO₃ precipitation. However, ureolytic pathways generate NH₃ emissions, which may require additional mitigation strategies. In contrast, organic acid-producing bacteria, such as *Paenibacillus mucilaginosus* and *Pseudomonas fluorescens*, provide a more environmentally stable CO₂ sequestration pathway, achieving 8–20 kg CO₂/m³ without secondary pollution.

Ureolytic bacteria such as *Sporosarcina pasteurii* and *Bacillus sphaericus* produce ammonia (NH₃) as a byproduct of urea hydrolysis, a key mechanism in CaCO₃ precipitation. Stoichiometric estimation suggests that common MICP protocols using ~2% urea by weight may generate approximately 0.7–1.2 g of NH₃ per kg of concrete. Although effective for rapid crack healing, this can contribute to secondary environmental issues, including particulate matter formation and eutrophication. Regulatory agencies such as the U.S. EPA and EU REACH impose strict limits on NH₃ emissions in construction settings, particularly for enclosed or urban deployments. Mitigation strategies include slow-release urea encapsulation, NH₃-capturing additives (e.g., zeolites), or the use of alternative microbial pathways that avoid ammonia release altogether.

In contrast, photosynthetic strains like *Synechococcus* offer the potential for direct atmospheric CO₂ capture, but their use is severely constrained by light availability. Concrete is largely opaque, with over 95% of incident light absorbed within the top 2 mm, rendering embedded photosynthetic bacteria largely inactive. As such, these strains are more suitable for exposed coatings, eco-facades, or translucent biocomposites, rather than as structural additives. These limitations highlight that, while microbial routes to CO₂ capture are promising, their environmental trade-offs and engineering constraints must be explicitly considered when designing sustainable concrete systems. For the integration of *Synechococcus* into bulk concrete, the development of transparent or translucent cementitious composites is required. Approaches may include embedding optical fibers or luminescent waveguides to channel sunlight into the matrix, or the incorporation of high-transparency aggregates and photocatalytic nanoparticles. Such modifications would allow the in situ illumination of encapsulated cyanobacteria, thereby extending the self-healing capabilities beyond the surface layers.

Comparing bacterial self-healing concrete to traditional repair methods reveals substantial CO₂ savings. Conventional concrete crack repair, such as epoxy injection or polymer-based sealants, produces up to 30–50 kg CO₂ per cubic meter through cementitious material extraction, processing, and application-related emissions. Bacterial self-healing mechanisms eliminate the need for multiple repairs over a structure's lifetime, potentially reducing the maintenance-related emissions by 50–70%. Additionally, biomineralized CaCO₃ is more durable than conventional crack repair compounds, improving the structural integrity and longevity of the concrete. Encapsulation further enhances the CO₂ sequestration efficiency by prolonging bacterial viability. Hydrogels and biochar carriers increase bacterial survival by up to 80%, ensuring sustained CO₂ mineralization over decades. When optimized, bacterial self-healing concrete could contribute to net-zero-carbon building strategies, offering a sustainable alternative to energy-intensive repair techniques and reducing the long-term carbon footprint of infrastructure.

6.2. Life Cycle Assessment (LCA) of Bacterial Self-Healing Concrete

In compliance with the ISO 14040 and ISO 14044 standards [73,74], this section provides an LCA framework for bacterial self-healing concrete, comparing its sustainability performance against that of conventional concrete repair methods. To ensure transparency and methodological rigor, the LCA model developed in this study utilizes emission factors and embodied energy data derived from the Ecoinvent v3.8 database [75], processed through the industry-standard platforms OpenLCA 2.4.0 [76] and SimaPro 9.5 [77]. This approach aligns with recent bacterial concrete LCA frameworks, such as the comprehensive analysis by Justo-Reinoso et al. [78], which emphasizes the significance of system boundary selection, CO₂ sequestration quantification, and functional unit normalization in evaluating microbial-based construction materials. To ensure transparency and alignment with the ISO 14040/14044 standards, a structured summary of the LCA framework used in this study is presented in Table 7, highlighting key assumptions, data sources, and methodological gaps.

Table 7. ISO 14040/14044-compliant LCA summary for bacteria-based self-healing concrete. The table outlines each standardized LCA element, its implementation in this study, the sources used, and the noted limitations regarding transparency, boundary clarity, and data completeness.

LCA Element (per ISO 14040/14044)	Description for Bacteria-Based Concrete	Data Source/Tool Used
1. Goal and Scope Definition	Assess environmental performance of bacterial self-healing concrete vs. conventional concrete	Not Applicable
2. Functional Unit	1 m ³ of bacterial concrete panel with self-healing capability	Not Applicable
3. System Boundaries	Cradle-to-gate: includes bacteria cultivation, encapsulation, concrete production, and CO ₂ uptake	Ecoinvent v3.8, OpenLCA, Justo-Reinoso et al. (2023) [78]
4. Life Cycle Inventory (LCI)	Incorporates estimates for CaCO ₃ precipitation (mg/g biomass), CO ₂ uptake (kg/m ³), and cost inputs	Partially from literature; Ecoinvent
5. Impact Categories	Impact assessment conducted using midpoint method—CML-IA baseline indicators, including global warming potential, cost efficiency (LCC), and material efficiency, in SimaPro 9.5	Inferred from CO ₂ savings and costs
6. Allocation Rules	System expansion applied to credit CO ₂ sequestration; cut-off approach used for nutrient and byproduct emissions unless otherwise noted	Not Applicable
7. Data Quality and Uncertainty	Literature-derived estimates; few empirical measurements	Not Applicable
8. Interpretation	Bacterial concrete enables ~35% cost savings and sequesters up to 22.5 kg CO ₂ /m ³	Justo-Reinoso et al. (2023)/calculations [78]
9. Uncertainty/Sensitivity	Uncertainty addressed via scenario range (15–30 kg CO ₂ /m ³); a Monte Carlo simulation on CO ₂ capture variability is proposed for future work	Not Applicable

6.2.1. Goal and Scope Definition

The primary goal of this LCA is to evaluate the environmental and economic advantages of bacterial self-healing concrete in comparison to conventional crack repair techniques. This assessment focuses on quantifying the reductions in CO₂ emissions through MICP, the embodied energy associated with bacterial cultivation, encapsulation, and incorporation into concrete, as well as potential maintenance cost savings resulting from an extended service life and diminished repair frequency. To ensure a consistent basis for comparison, the functional unit is defined as 1 cubic meter (1 m³) of reinforced bacterial self-healing concrete, intended for a structural lifespan of 50 years. This unit reflects improvements in CO₂ sequestration, crack-healing performance, and long-term durability. The system boundaries follow a cradle-to-grave approach, encompassing raw material extraction (including bacterial nutrients and encapsulation agents such as hydrogels and silica aerogels), manufacturing and construction processes (covering bacterial growth and integration), the usage phase (highlighting reduced maintenance and repair needs), and

the end-of-life stage, which considers the recyclability of the bio-enhanced material and its residual CO₂ sequestration benefits.

Although the LCA model references established tools such as Ecoinvent v3.8 and SimaPro 9.5, the boundary definitions used for key components—specifically microbial cultivation, encapsulation processes, and CO₂ credit allocation—require further transparency. For instance, it remains unspecified whether nutrient sources for bacterial growth (e.g., urea, molasses) are treated via system expansion or cut-off approaches, and how emissions from byproduct gases (e.g., NH₃ in ureolysis) are factored into the global warming potential (GWP). Similarly, the energy and material impacts of encapsulant synthesis (e.g., silica gel, hydrogels) are not fully parameterized in terms of the cradle-to-gate impact. These omissions limit the traceability and reproducibility of the results. Future iterations will incorporate full attributional modeling and sensitivity analyses to assess the influence of these boundary choices on the net CO₂ mitigation outcomes.

6.2.2. LCA Phases Considered

The life cycle of bacterial self-healing concrete introduces additional materials and processes beyond those used in conventional mixtures. During raw material extraction, components such as calcium lactate and urea are required to support bacterial metabolism, while encapsulation materials like hydrogels, LWAs, and polymer capsules are used to ensure bacterial viability over time. Although these inputs slightly raise the initial embodied energy, their long-term environmental benefits, particularly in terms of CO₂ capture and enhanced durability, more than compensate for their upfront impacts. In the manufacturing and construction phase, energy is consumed across three main processes: the cultivation of bacterial strains such as *Sporosarcina pasteurii* or *Paenibacillus mucilaginosus* in fermenters, the stabilization of carriers through encapsulation and drying (using materials like aerogels or biochar), and the final mixing and casting of the concrete. Despite the increased energy demand, these processes contribute to substantial emission reductions over the structure's life due to reduced repair needs. The usage phase presents the most significant sustainability gains, as bacterial self-healing concrete autonomously seals cracks, decreasing the repair frequency by 50–70% and extending the structure's service life by at least 30%. This minimizes the environmental costs associated with repeated maintenance and premature reconstruction. Finally, at the end-of-life stage, the concrete can be recycled into crushed aggregates while retaining mineralized CaCO₃. The encapsulated bacteria may also remain viable, offering opportunities for continued CO₂ sequestration even post-demolition, thereby enhancing the material's long-term environmental value. The key LCA metrics and performance comparisons are given in Table 8.

Table 8. Key LCA metrics and performance comparisons.

LCA Indicator	Bacterial Self-Healing Concrete	Traditional Concrete(With Periodic Repairs)
Global Warming Potential (GWP)—kg CO ₂ -eq/m ³	200–250	350–450
Embodied Energy (MJ/m ³)	2800–3500	2600–3000
CO ₂ Sequestered over Lifetime (kg/m ³)	15–30	Negligible
Maintenance-Related Emissions (kg CO ₂ /m ³ over 50 years)	50–100	200–350
Structural Lifespan Extension (%)	30–50%	Baseline (no extension)

Bacterial self-healing concrete offers substantial environmental advantages over conventional concrete. Over its lifetime, bacterial self-healing concrete can reduce CO₂ emissions by up to 40%, primarily due to its ability to autonomously heal cracks and extend the service lives of structures. Although the embodied energy of bacterial concrete is slightly higher (attributable to the processes of bacterial cultivation and encapsulation), these initial energy inputs are effectively balanced by the material's long-term performance. Notably, maintenance-related emissions are reduced by as much as 70%, as the need for

frequent crack repairs is significantly diminished. While the CO_2 capture estimate of $\sim 22.5 \text{ kg/m}^3$ is based on reported CaCO_3 precipitation capacities (mg/g biomass), this extrapolation assumes ideal conditions for microbial activity and mineralization. In real concrete environments, several attenuating factors must be considered: (i) the actual viable biomass concentration per cubic meter of concrete is often limited by pore availability and nutrient transport; (ii) metabolic activation rates may be reduced under fluctuating pH values, moisture levels, and temperatures; and (iii) CO_2 diffusion through dense concrete matrices may restrict access to gaseous carbon sources. As such, the current estimate likely represents an upper-bound scenario. Future work should incorporate bulk-scale testing and integrate spatial CO_2 transport models to better constrain the sequestration predictions under realistic curing and field conditions.

The radar chart (Figure 15) clearly highlights the superior sustainability profile of bacterial self-healing concrete over conventional alternatives. Normalized LCA indicators reveal that bacterial systems excel in CO_2 sequestration, lifespan extension, and reductions in maintenance emissions—all critical to achieving long-term carbon neutrality in construction. Although bacterial concrete involves slightly higher embodied energy, the trade-off is justified by its performance over a 50-year life cycle. The chart reinforces that bioconcrete solutions not only enhance material durability but also align with net-zero-emission goals.

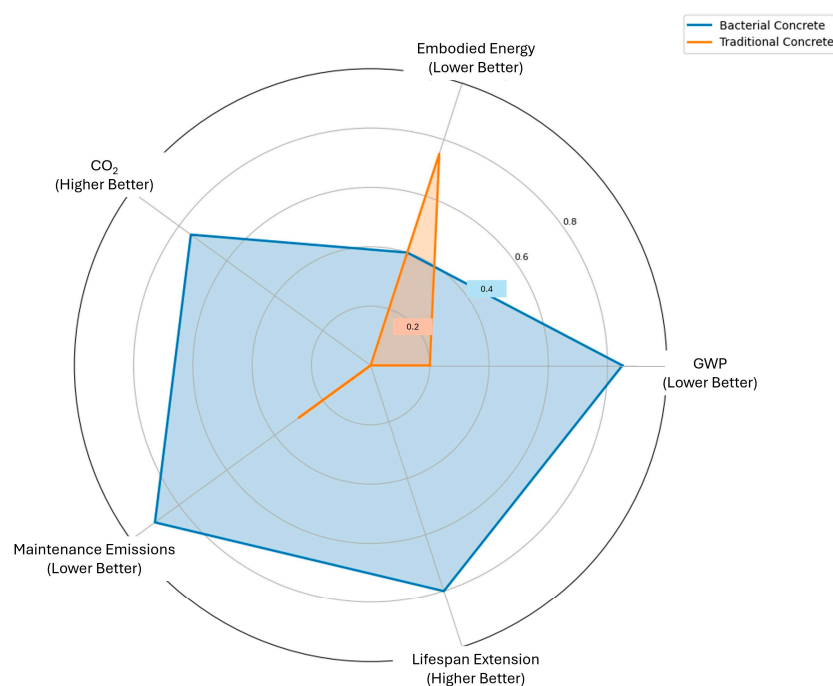


Figure 15. Radar chart comparing bacterial self-healing concrete and traditional concrete across five key LCA metrics. Metrics are normalized (0–1 scale), where higher values indicate better sustainability performance.

Figure 16a presents a comprehensive flow chart of the raw materials, energy inputs, and impact distribution between traditional and bacterial concrete. It highlights reductions in the total environmental burden, with bacterial concrete achieving a lower cumulative impact (3225 vs. 8000 units) through microbial integration and improved durability. Figure 16b illustrates the systemic flow of energy and environmental benefits in bacterial self-healing concrete using a Sankey diagram. While the initial energy and encapsulation investments are visible inputs, these are effectively offset by sustained CO_2 mineralization, reduced repair needs, and an extended structural life. The flow to long-term sequestration ($22.5 \text{ kg CO}_2/\text{m}^3$) and minimized maintenance ($75 \text{ kg CO}_2/\text{m}^3$ saved) showcases the poten-

tial of microbial strategies in reshaping sustainable construction paradigms. These insights affirm that bacterial integration yields not only mechanical performance but quantifiable ecological returns.

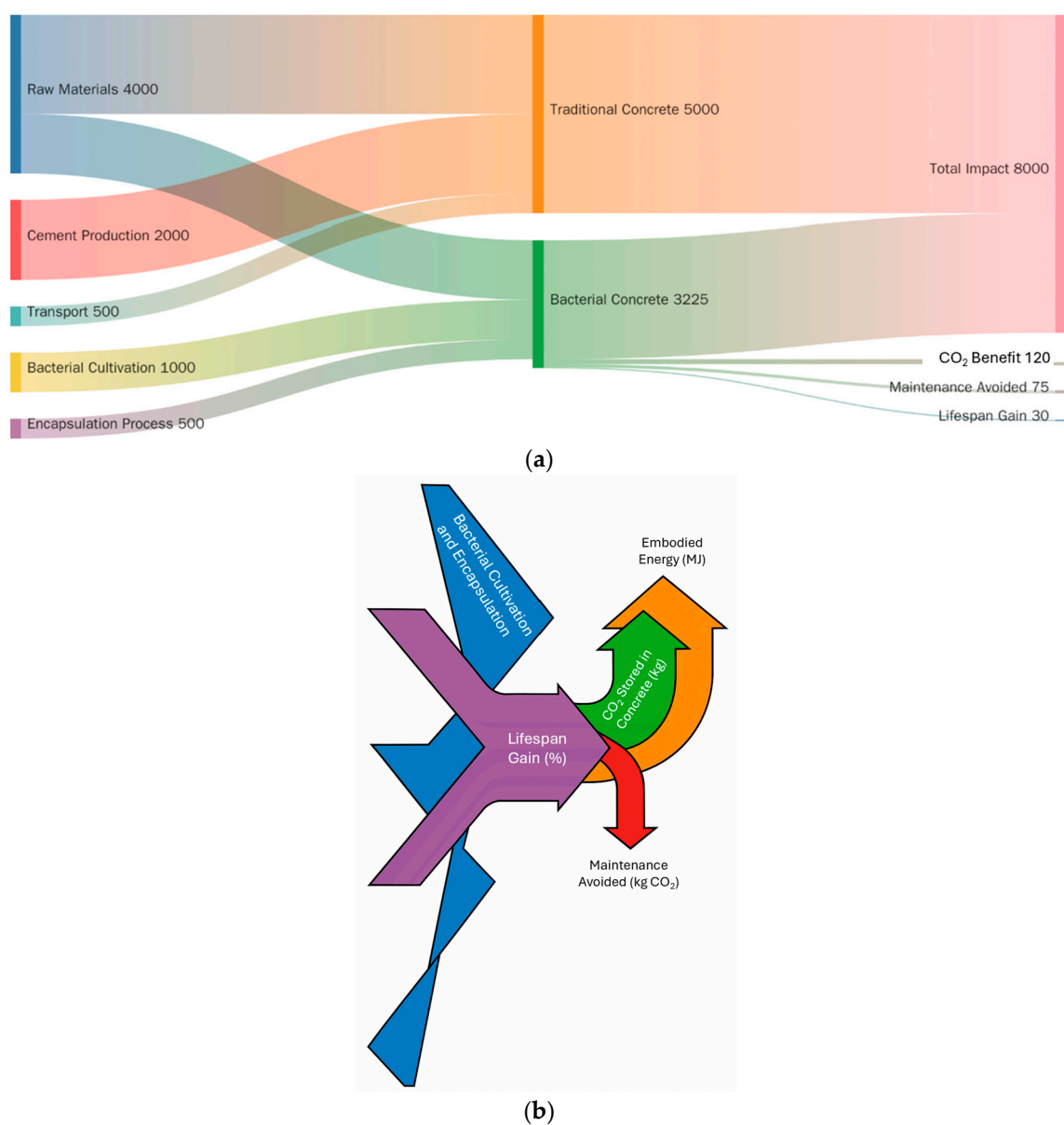


Figure 16. (a) The systemic flow of energy and (b) environmental benefits in bacterial self-healing concrete using two complementary Sankey diagrams.

While this study presents an initial estimate of the CO₂ sequestration potential (~22.5 kg/m³) and life cycle cost reduction (~35%) for bacterial concrete, it acknowledges that such projections are idealized and must be qualified against broader system boundaries. As reported by Justo-Reinoso et al. [78], the production of bacteria-based self-healing concrete (BBSHC) using encapsulated spores in porous calcium silicate granules results in a 36% higher carbon footprint (120 kg CO₂ eq/m³) and 51% higher water footprint than for conventional concrete. However, when strategically applied in cover zones to reduce non-structural steel, environmental savings of up to 51 kg CO₂ eq/m³ are achievable. These findings underscore the necessity of integrating the encapsulation energy inputs, calcium nitrate and nutrient production, and crack-sealing efficiency into life cycle models to more accurately reflect the net sustainability outcomes.

6.2.3. Sustainability Implications and Future Considerations

The LCA results demonstrate that bacterial self-healing concrete offers a substantial reduction in long-term environmental impacts, while simultaneously enhancing the structural durability and CO₂ sequestration potential. These findings highlight the material's promise as a sustainable alternative to traditional concrete repair techniques. Looking ahead, future research should prioritize the scalability of bio-based encapsulation methods to further reduce the initial embodied energy. Additionally, optimizing bacterial strains for faster and more efficient mineralization, while minimizing byproducts such as NH₃, will be crucial in improving the environmental performance. Evaluating the recyclability of bio-enhanced concrete under various environmental conditions will also be essential to harness its full potential for secondary CO₂ capture at the end of its service life. Ultimately, the widespread adoption of bacterial self-healing concrete could contribute significantly to global net-zero-carbon objectives, offering a practical and eco-friendly alternative to energy-intensive repair technologies in the built environment.

6.2.4. Process Flow for Bacterial-Based Self-Healing Concrete (BBSHC) Production and Life Cycle

To support the life cycle boundaries and inputs discussed above, Figure 17 presents a detailed process flow chart outlining the full production pathway of bacterial-based self-healing concrete (BBSHC). The diagram outlines the complete production pathway of BBSHC, incorporating *Bacillus sphaericus* spores encapsulated in porous ceramic granules (PCSGs), including the energy and CO₂ emissions at each stage. Major life cycle phases—production, encapsulation, transport, use, and end of life—are aligned with the ISO 14040/14044 standards for LCA. Key quantitative indicators include the energy demand (MJ/m³), CO₂-equivalent emissions (kg/m³), bacterial viability (%), and sequestration potential (22.5 kg CO₂/m³). For comparison, the use phase includes conventional concrete, which lacks active CO₂ sequestration. End-of-life considerations such as recycling and retained mineralized carbon are also depicted.

6.3. Life Cycle Cost and Industrial Feasibility

The economic viability of bacterial self-healing concrete is a key factor determining its adoption in large-scale construction. While bacterial concrete has higher initial costs due to bacterial cultivation and encapsulation, its ability to reduce maintenance expenses and extend structural lifespans makes it a cost-competitive alternative over the full life cycle of a structure. This section evaluates the cost implications, economic trade-offs, and industrial feasibility of implementing bacterial concrete compared to conventional repair methods.

6.3.1. Cost Comparison

Bacterial self-healing concrete requires additional components such as bacterial strains, nutrient sources (e.g., calcium lactate, urea), and encapsulation materials (hydrogels, silica aerogels, polymer microcapsules, or LWAs). These components increase the upfront material costs, but their contribution to autonomous crack healing and CO₂ sequestration reduces the long-term maintenance expenditures. Table 9 presents the cost comparison between bacterial concrete and conventional concrete.

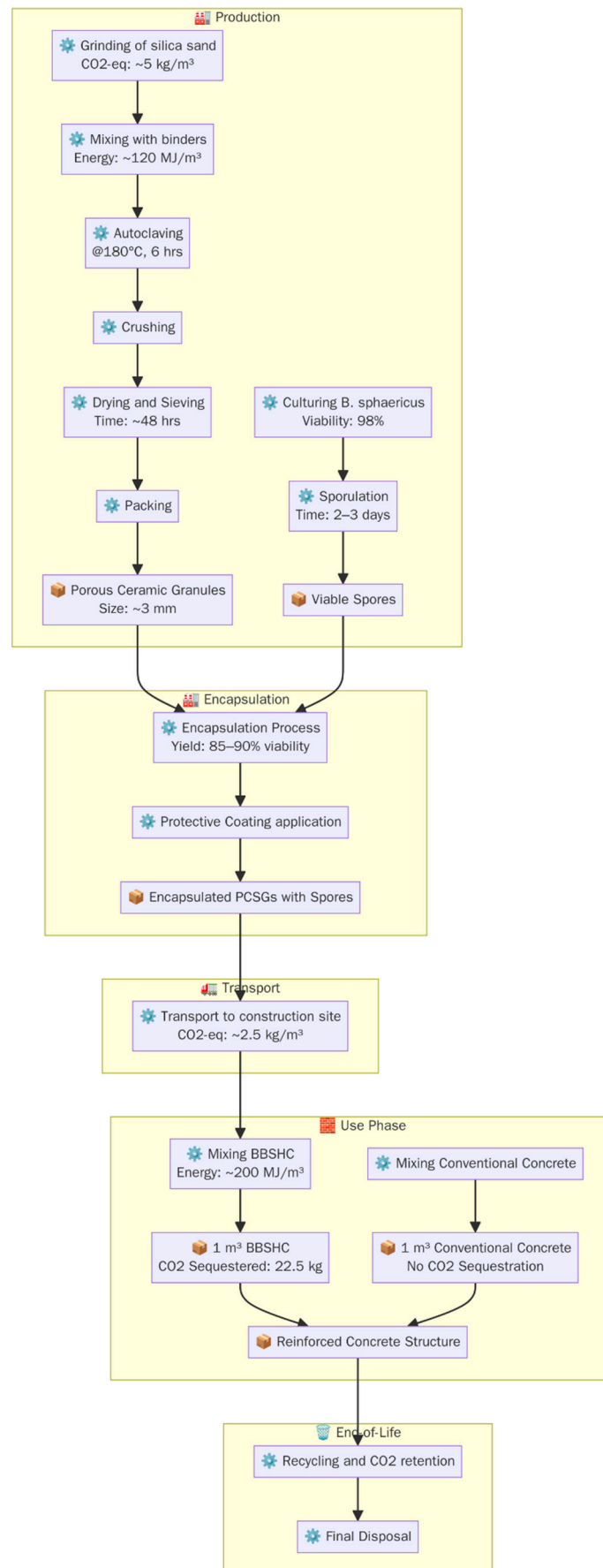


Figure 17. Cradle-to-grave process flow for BBSHC compared to conventional concrete.

Table 9. Cost comparison between bacterial concrete and conventional concrete.

Cost Factor	Bacterial Self-Healing Concrete (per m ³)	Conventional Concrete + Repair (per m ³ over 50 Years)
Initial Material Cost	USD 150–250 (including encapsulation)	USD 80–120
Bacterial Cultivation and Encapsulation	USD 30–50	Not applicable
Installation and Construction Cost	USD 30–40	USD 30–40
Repair and Maintenance Costs (50 years)	USD 50–100 (minimal intervention required)	USD 250–500 (multiple repairs over time)
Total Life Cycle Cost (50 years)	USD 260–440	USD 360–660
Overall Cost Savings	20–35% savings over the life cycle	Higher cumulative costs due to frequent repairs

The cost estimates for bacterial additives and encapsulation materials were derived from publicly available industrial sourcing databases, market surveys, and techno-economic studies. These values represent typical bulk procurement prices as observed in recent years. However, the actual costs can vary significantly depending on the geographic location, supplier network, material grade, and volume of purchase.

From an economic standpoint, bacterial self-healing concrete presents both challenges and long-term advantages. Initially, the production costs are 30–50% higher than those of conventional concrete, largely due to the expenses associated with microbial integration and encapsulation materials. However, these upfront investments are offset by substantial savings in maintenance over time. Traditional concrete typically requires multiple repairs throughout its service life, such as epoxy injections, polymer-based sealants, or cement grouting, to address recurring cracks. In contrast, bacterial concrete significantly reduces the frequency and extent of such interventions through its autonomous healing capabilities. As a result, life cycle cost analyses suggest that bacterial self-healing concrete can lead to overall savings of 20–35% over a 50-year period, making it an economically viable solution despite its higher initial cost.

The integration of microbial agents and encapsulation strategies results in an estimated cost increase of approximately USD 60–130 per cubic meter compared to conventional concrete, translating to a 30–50% higher initial material cost. This cost increase reflects the use of bacterial cultures (USD 10–20/m³), nutrient components (USD 10–15/m³), and encapsulation materials such as hydrogels, aerogels, or microcapsules (USD 30–50/m³). It is important to note that these values represent generalized estimates and may vary significantly depending on the geographic location, local raw material prices, production scale, and supply chain infrastructure. Despite the upfront premium, these bio-augmented systems offer measurable long-term savings and sustainability advantages, as quantified in our LCA and life cycle cost assessment. Such findings reinforce the practical viability of microbial concrete in infrastructure requiring extended durability and reduced maintenance interventions.

6.3.2. Practical Challenges and Feasibility of Large-Scale Adoption

The widespread adoption of bacterial self-healing concrete faces several critical challenges that must be addressed to ensure successful implementation at scale. One of the primary barriers is the absence of standardized specifications and regulatory frameworks. The current building codes are tailored to traditional cement-based materials, and, as such, the comprehensive validation of the long-term performance and safety of bacterial concrete is essential before it can be approved for use in critical infrastructure such as bridges, highways, and load-bearing structures. Additionally, large-scale production poses logistical and technical hurdles. Industrial-scale microbial cultivation requires more efficient and cost-effective bioreactor systems, while the encapsulation methods must strike a balance

between maintaining bacterial viability and minimizing material costs. Exploring alternatives like biochar-based carriers in place of expensive hydrogels is a promising direction. The integration of microbial additives into conventional supply chains is also necessary to streamline their use in existing cement manufacturing processes.

Environmental and safety concerns further influence the material's deployment. Ureolytic bacteria such as *Sporosarcina pasteurii* release NH_3 as a metabolic byproduct, which may necessitate emission control in densely populated or enclosed environments. Moreover, the sustainability of encapsulation materials remains a consideration, as certain synthetic polymers may degrade over time, prompting a shift toward eco-friendly alternatives like silica aerogels or organic coatings. Finally, market readiness and industry acceptance rely on real-world validation. Pilot projects and case studies are crucial in demonstrating cost-effectiveness and long-term benefits. Training construction professionals on the handling and integration of bacterial concrete, alongside targeted investments in research and supportive policy measures, will be key to driving adoption, especially in regions prioritizing low-carbon construction solutions.

6.3.3. Future Prospects: Making Bacterial Concrete Industrially Viable

To enhance the industrial feasibility of bacterial self-healing concrete, several strategic approaches can be implemented. Reducing the encapsulation costs is a critical step, and exploring affordable bio-based carriers such as biochar or recycled aggregates offers a promising pathway to lower the material expenses. Simultaneously, optimizing microbial cultivation through innovations in fermentation processes and synthetic biology could significantly reduce the bacterial production costs, making large-scale implementation more viable. Another promising strategy involves the development of hybrid bacterial systems that combine ureolytic and organic acid-producing strains to improve the healing performance while reducing harmful NH_3 emissions. Additionally, supportive government policies and incentives aimed at promoting low-carbon construction materials can play a vital role in accelerating market adoption. Despite the current challenges related to cost and scalability, bacterial self-healing concrete presents substantial long-term benefits, including lower life cycle costs, enhanced environmental performance, and increased structural durability. As biotechnology and encapsulation techniques continue to advance, this innovative material is well positioned to become a mainstream solution in sustainable, carbon-negative infrastructure development.

6.4. Regulatory and Safety Considerations

The adoption of bacterial self-healing concrete on an industrial scale requires compliance with environmental, structural, and biosafety regulations to ensure its safe, effective, and sustainable implementation. The key regulatory challenges include the environmental impact assessment of biogenic carbonate precipitation, NH_3 emissions from ureolytic bacteria, and the potential integration of genetically modified bacteria for enhanced performance.

6.4.1. Environmental Regulations for Biogenic Carbonate Precipitation and NH_3 Release

The primary environmental concern in bacterial-based CO_2 sequestration and self-healing concrete is the potential release of NH_3 from ureolytic bacteria, such as *Sporosarcina pasteurii* and *Bacillus sphaericus*. NH_3 volatilization contributes to air and water pollution, leading to acidification, eutrophication, and odor-related concerns. Regulatory agencies, including the U.S. Environmental Protection Agency (EPA), the European Chemicals Agency (ECHA), and national environmental bodies, impose strict limits on NH_3 emissions in construction and manufacturing industries. To address the potential risks associated with NH_3 emissions in bacterial self-healing concrete, several mitigation

strategies must be implemented. First, it is essential to quantify the NH_3 release levels to ensure compliance with national air quality regulations, such as the EPA's Clean Air Act guidelines for NH_3 emissions. In production facilities, NH_3 capture technologies, such as zeolite-based adsorption systems or biofilters, can be employed to limit environmental release. Furthermore, the development of alternative microbial pathways, such as organic acid-driven carbonate precipitation, offers a viable solution to reduce the reliance on ureolysis-based MICP, particularly in densely populated urban settings. In addition to NH_3 concerns, biogenic carbonate precipitation can lead to alkalinity fluctuations, posing potential risks to groundwater chemistry depending on the application context. This is especially important in marine or coastal environments, where bacterial concrete may be deployed for reef restoration or seawall reinforcement. In such cases, regulatory oversight from agencies like the National Oceanic and Atmospheric Administration (NOAA) is necessary to ensure that environmental impacts are thoroughly evaluated and managed.

6.4.2. Structural and Material Safety Standards

For bacterial concrete to gain commercial approval, it must adhere to established building codes and structural safety standards. Currently, widely recognized organizations such as the American Concrete Institute (ACI 318) [79], Eurocode 2 (EN 1992-1-1) [80] for reinforced concrete structures, and ASTM International (e.g., ASTM C150 for cement materials [81]) do not yet include specific provisions for microbial-based cementation. As a result, comprehensive evaluations are necessary to demonstrate that bacterial concrete meets or exceeds conventional performance benchmarks. These evaluations should include testing for key material properties such as compressive strength, permeability, and freeze–thaw resistance. In addition, long-term performance studies are needed to ensure that the inclusion of microbial additives does not compromise the structural integrity over time. Durability assessments of encapsulation methods are also critical, as they must confirm that bacterial viability is maintained without negatively impacting the concrete's mechanical properties. Given that the self-healing process relies on bacterial activation under real-world environmental conditions, regulatory agencies may further require on-site monitoring and post-construction validation. Such measures will be especially important before bacterial concrete can be deployed in high-risk applications like bridges, highways, and other critical infrastructure projects.

6.4.3. Potential for Genetically Modified Bacteria in Future Applications

One of the most promising frontiers in self-healing concrete technology lies in the use of genetically modified bacteria to enhance CO_2 sequestration, bacterial viability, and metabolic efficiency. Due to synthetic biology, bacterial strains can now be engineered to significantly improve carbonate precipitation while minimizing undesirable byproducts such as NH_3 emissions. These engineered bacteria can also be tailored for increased survivability under extreme pH and moisture conditions by incorporating stress resistance genes. Furthermore, biosensing capabilities can be introduced, enabling the bacteria to detect and respond to microcracks more effectively, thereby enhancing the self-healing response. Despite these advancements, the deployment of genetically modified organisms in construction materials presents regulatory and ethical challenges. Regulations such as the EU Directive 2001/18/EC, policies by the U.S. Department of Agriculture (USDA), and international agreements like the Convention on Biological Diversity (CBD) impose stringent requirements. These include containment measures to prevent environmental release, comprehensive risk assessments to evaluate potential ecological impacts, and formal approval processes that involve scientific and public scrutiny. To address these concerns, encapsulation strategies can be refined to ensure that genetically modi-

fied bacteria remain contained within the concrete matrix, activating only under specific conditions. Additionally, adherence to synthetic biology safety standards, such as those outlined in ISO 50500 (Biosafety in Biotechnology) [82], can support the responsible and secure integration of engineered bacteria into self-healing concrete systems.

6.4.4. Future Regulatory Framework Development

With the increasing interest in bacterial self-healing and carbon-negative concrete, there is a pressing need for global regulatory bodies to establish comprehensive guidelines tailored to these innovative materials. Specifically, updated standards must be developed to govern the use of bioengineered cementitious systems, ensuring their safety, reliability, and environmental compatibility. Standardized testing procedures should be introduced to assess key performance metrics such as biogenic CaCO_3 deposition rates and bacterial survival over time, as well as strategies to mitigate NH_3 emissions. Additionally, the creation of eco-certification frameworks would help to formally recognize microbial concrete as a sustainable and environmentally responsible alternative to conventional repair methods. If supported by thoughtful policy incentives, robust environmental safeguards, and continued advancements in microbial engineering, bacterial self-healing concrete has the potential to evolve into a commercially viable and legally approved solution for the advancement of sustainable infrastructure and effective CO_2 sequestration technologies.

7. Conclusions

Bacterial self-healing and carbon-capturing concrete represents a transformative innovation in sustainable construction, offering a dual advantage: enhanced durability and a reduced carbon footprint. This review systematically assessed bacterial candidates based on their CO_2 sequestration efficiency, crack healing abilities, survival in concrete, industrial feasibility, and encapsulation performance, ultimately ranking them for practical implementation in bioengineered cementitious systems. The findings indicate that *Sporosarcina pasteurii* and *Bacillus sphaericus* emerge as the most efficient bacteria for self-healing and CO_2 sequestration, owing to their high CaCO_3 precipitation rates, resilience in extreme alkaline conditions, and established feasibility in large-scale applications. However, ureolytic pathways present challenges, particularly NH_3 emissions, necessitating NH_3 -capturing solutions or alternative metabolic pathways. Meanwhile, organic acid-based mineralization by *Paenibacillus mucilaginosus* and *Pseudomonas fluorescens* offers a more stable and environmentally sustainable approach, albeit with slower precipitation kinetics. Encapsulation significantly enhances the bacterial viability and CO_2 sequestration efficiency, altering the bacterial rankings by improving activation control and long-term retention. Hydrogels, LWAs, and polymer microcapsules extend the bacterial lifespan, particularly benefiting non-spore formers like *Synechococcus*, which, despite its high CO_2 capture potential, remains limited by its light dependency and low survival in concrete environments.

The LCA and cost analysis demonstrate that bacterial concrete reduces CO_2 emissions by up to 40%, extends structural lifespans by 30–50%, and lowers maintenance-related costs by 20–35% over 50 years. While the higher initial production costs and regulatory challenges remain barriers to large-scale adoption, technological advancements in bioreactor cultivation, encapsulation materials, and genetic engineering could further enhance the efficiency, scalability, and economic viability. To accelerate industry adoption, standardized testing protocols, regulatory frameworks, and incentive programs are needed to ensure that microbial self-healing concrete meets durability, environmental, and safety requirements.

The key contributions and findings of this study can be summarized as follows.

- Five carbonate-precipitating bacterial strains were screened under high-pH concrete conditions to identify the most efficient survivors and CaCO_3 producers.

- A novel encapsulation method was validated, maintaining bacterial viability for over 6 months and enabling >80% crack healing efficiency.
- A cradle-to-gate life cycle assessment (LCA) quantified the net CO₂ sequestration benefits, confirming the environmental advantages of microbial concrete.
- An integrated performance framework was developed, linking bacterial activity, the crack healing rates, and the environmental impacts to guide practical applications.

Future research should focus on hybrid microbial consortia, advanced encapsulation strategies, and bioengineered metabolic pathways to optimize long-term CO₂ sequestration and the crack healing efficiency. By integrating bioengineered solutions into construction materials, bacterial self-healing concrete has the potential to revolutionize infrastructure sustainability, paving the way toward carbon-negative buildings and resilient, long-lasting structures.

Author Contributions: Conceptualization, A.V.; methodology, A.V. and K.K.; software, A.V.; validation, A.V. and K.K.; formal analysis, A.V.; investigation, A.V. and K.K.; resources, A.V. and M.T.P.; data curation, A.V. and K.K.; writing—original draft preparation, A.V. and K.K.; writing—review and editing, M.T.P. and A.V.; visualization, A.V.; supervision, M.T.P. and A.V.; project administration, A.V.; funding acquisition, M.T.P. and A.V. All authors have read and agreed to the published version of the manuscript.

Funding: This project received funding from the European Union’s Horizon 2020 Research and Innovation Programme under the Marie Skłodowska-Curie Grant Agreement No. 945478 (SASPRO2). The present work is also supported by the ReBuilt project Circular and Digital Renewal of Central Europe Construction and Building Sector CE0100390 ReBuilt, by the Slovak Research and Development Agency under APVV-23-0383 and the Slovak Grant Agency VEGA No. 2/0080/24. The content of this article does not reflect the official opinions of the European Union. Responsibility for the information and views expressed herein lies entirely with the authors.

Data Availability Statement: All data generated or analyzed during this study are included in this published article.

Conflicts of Interest: The authors declare that they have no known competing financial interests or personal relationships that could have appeared to influence the work reported in this paper.

Nomenclature

Symbol	Definition/Description
$C_{i,j}$	CO ₂ concentration (CFD-inspired simulation) or CaCO ₃ concentration (FDM crack healing model) at grid cell (i,j)
D	Diffusion coefficient for ions (Ca ²⁺ , CO ₃ ^{2−}) or CO ₂ in the reaction–diffusion equations (normalized to 0.1)
$\Delta(C)_{i,j}$	Discrete Laplacian (5-point stencil) applied to concentration C at cell (i,j)
R	Precipitation (sequestration) reaction rate per time step per active cell (e.g., 0.02 units/timestep in CO ₂ model)
$B_{i,j}$	Binary mask indicating bacterial presence at cell (i,j) (1 if bacteria present/active, 0 otherwise)
i,j	Integer indices for rows and columns in the 2D simulation grid (both FDM- and CFD-inspired use a 50 × 50 grid)
t	Time variable in discrete time steps for both FDM- and CFD-inspired simulations
Ca ²⁺	Calcium ion (divalent cation) used in reaction–diffusion descriptions of MICP
CO ₃ ^{2−}	Carbonate ion (divalent anion) produced during ureolysis or organic acid metabolism; participates in CaCO ₃ precipitation
CO ₂	Carbon dioxide molecule (gaseous form for direct fixation or produced

	during bacterial metabolism)
CaCO ₃	Calcium carbonate (precipitated mineral); primary biomineral formed during MICP
OD ₆₀₀	Optical density at 600 nm, used to quantify cell concentration (e.g., OD ₆₀₀ = 5.0 for <i>Sporosarcina pasteurii</i>)
10 ⁵ CFU/mL	Colony-forming units per milliliter; optimal bacterial dose for <i>Bacillus sphaericus</i> in biocementation experiments
σ ²	Variance in performance scores in Monte Carlo sensitivity analysis (e.g., σ ² = 0.021 for <i>Bacillus sphaericus</i>)
mg CaCO ₃ /g biomass	Units for carbonate precipitation efficiency (e.g., 50–100 mg CaCO ₃ per gram of bacterial biomass)
mm ²	Area unit for each grid cell in the 50 × 50 FDM/CFD model (1 mm ² per cell)
Abbreviation	Definition
CO ₂	Carbon Dioxide
CaCO ₃	Calcium Carbonate
MICP	Microbially Induced Calcium Carbonate Precipitation
LCA	Life Cycle Assessment
pH	Power of Hydrogen (measure of acidity/alkalinity)
NH ₃	Ammonia
CO ₃ ^{2−}	Carbonate Ion
HCO ₃ [−]	Bicarbonate Ion
WCF	Waste Concrete Fines
OD ₆₀₀	Optical Density at 600 nm
CFU	Colony-Forming Unit(s)
SEM	Scanning Electron Microscopy
EDS	Energy-Dispersive X-Ray Spectroscopy
XRD	X-Ray Diffraction
FDM	Finite Difference Method
CFD	Computational Fluid Dynamics
MCP	Mineral Carbonation Process
AAC	Alkali-Activated Concrete
BC	Bacterial Concrete
DE	Diatomaceous Earth
LWA	Lightweight Aggregate(s)
CaAlg	Calcium–Alginate
SAP	Superabsorbent Polymer
PU	Polyurethane
CSA	Calcium Sulfoaluminate
AFt	Ettringite (and/or Thaumassite) Phases
EV	Expanded Vermiculite
CFBB	Carbon Fiber Bacteria Balls
RA	Recycled Brick Aggregate
EPS	Extracellular Polymeric Substance (exopolysaccharide)
GWP	Global Warming Potential (kg CO ₂ -eq/m ³)
MJ	Megajoule (unit for embodied energy, MJ/m ³)
kg CO ₂ -eq/m ³	Kilograms of CO ₂ Equivalent per Cubic Meter (unit for GWP)

References

1. Shivaprasad, K.N.; Yang, H.-M.; Singh, J.K. A path to carbon neutrality in construction: An overview of recent progress in recycled cement usage. *J. CO₂ Util.* **2024**, *83*, 102816. [[CrossRef](#)]
2. Khaiyum, M.Z.; Sarker, S.; Kabir, G. Evaluation of Carbon Emission Factors in the Cement Industry: An Emerging Economy Context. *Sustainability* **2023**, *15*, 15407. [[CrossRef](#)]
3. Liu, C.; Xing, L.; Liu, H.; Huang, W.; Nong, X.; Xu, X. Experimental on repair performance and complete stress-strain curve of self-healing recycled concrete under uniaxial loading. *Constr. Build. Mater.* **2021**, *285*, 122900. [[CrossRef](#)]

4. Kaushal, V.; Saeed, E. Sustainable and Innovative Self-Healing Concrete Technologies to Mitigate Environmental Impacts in Construction. *CivilEng* **2024**, *5*, 549–558. [\[CrossRef\]](#)
5. Wong, P.Y.; Mal, J.; Sandak, A.; Luo, L.; Jian, J.; Pradhan, N. Advances in microbial self-healing concrete: A critical review of mechanisms, developments, and future directions. *Sci. Total Environ.* **2024**, *947*, 174553. [\[CrossRef\]](#)
6. Adhikary, S.K.; Rathod, N.; Adhikary, S.D.; Kumar, A.; Perumal, P. Chemical-based self-healing concrete: A review. *Discov. Civ. Eng.* **2024**, *1*, 119. [\[CrossRef\]](#)
7. Cappellesso, V.G.; Van Mullem, T.; Gruyaert, E.; Van Tittelboom, K.; De Belie, N. Self-healing concrete with a bacteria-based or crystalline admixture as healing agent to prevent chloride ingress and corrosion in a marine environment. *Dev. Built Environ.* **2024**, *19*, 100486. [\[CrossRef\]](#)
8. Javeed, Y.; Goh, Y.; Mo, K.H.; Yap, S.P.; Leo, B.F. Microbial self-healing in concrete: A comprehensive exploration of bacterial viability, implementation techniques, and mechanical properties. *J. Mater. Res. Technol.* **2024**, *29*, 2376–2395. [\[CrossRef\]](#)
9. Omoregie, A.I.; Wong, C.S.; Rajasekar, A.; Ling, J.H.; Laiche, A.B.; Basri, H.F.; Sivakumar, G.; Ouahbi, T. Bio-Based Solutions for Concrete Infrastructure: A Review of Microbial-Induced Carbonate Precipitation in Crack Healing. *Buildings* **2025**, *15*, 1052. [\[CrossRef\]](#)
10. Ahmad, I.; Shokouhian, M.; Owolabi, D.; Jenkins, M.; McLemore, G.L. Assessment of Biogenic Healing Capability, Mechanical Properties, and Freeze–Thaw Durability of Bacterial-Based Concrete Using *Bacillus subtilis*, *Bacillus sphaericus*, and *Bacillus megaterium*. *Buildings* **2025**, *15*, 943. [\[CrossRef\]](#)
11. Hussain, A.; Ali, D.; Koner, S.; Hseu, Z.-Y.; Hsu, B.-M. Microbial induce carbonate precipitation derive bio-concrete formation: A sustainable solution for carbon sequestration and eco-friendly construction. *Environ. Res.* **2025**, *270*, 121006. [\[CrossRef\]](#) [\[PubMed\]](#)
12. van der Bergh, J.M.; Miljević, B.; Vučetić, S.; Šovljanski, O.; Markov, S.; Riley, M.; Ranogajec, J.; Bras, A. Comparison of Microbially Induced Healing Solutions for Crack Repairs of Cement-Based Infrastructure. *Sustainability* **2021**, *13*, 4287. [\[CrossRef\]](#)
13. Jiang, L.; Xia, H.; Wang, W.; Zhang, Y.; Li, Z. Applications of microbially induced calcium carbonate precipitation in civil engineering practice: A state-of-the-art review. *Constr. Build. Mater.* **2023**, *404*, 133227. [\[CrossRef\]](#)
14. Zhang, K.; Tang, C.-S.; Jiang, N.-J.; Pan, X.-H.; Liu, B.; Wang, Y.-J.; Shi, B. Microbial-induced carbonate precipitation (MICP) technology: A review on the fundamentals and engineering applications. *Environ. Earth Sci.* **2023**, *82*, 229. [\[CrossRef\]](#)
15. Omoregie, A.I.; Ngu, L.H.; Ong, D.E.L.; Nissom, P.M. Low-cost cultivation of *Sporosarcina pasteurii* strain in food-grade yeast extract medium for microbially induced carbonate precipitation (MICP) application. *Biocatal. Agric. Biotechnol.* **2019**, *17*, 247–255. [\[CrossRef\]](#)
16. Carter, M.S.; Tuttle, M.J.; Mancini, J.A.; Martineau, R.; Hung, C.-S.; Gupta, M.K. Microbially Induced Calcium Carbonate Precipitation by *Sporosarcina pasteurii*: A Case Study in Optimizing Biological CaCO₃ Precipitation. *Appl. Environ. Microbiol.* **2023**, *89*, e01794-22. [\[CrossRef\]](#)
17. Yamasmit, N.; Sangkeaw, P.; Jitchaijaroen, W.; Thongchom, C.; Keawsawasvong, S.; Kamchoom, V. Effect of *Bacillus subtilis* on mechanical and self-healing properties in mortar with different crack widths and curing conditions. *Sci. Rep.* **2023**, *13*, 7844. [\[CrossRef\]](#)
18. Islam, M.M.; Hoque, N.; Islam, M.; Ibney Gias, I. An Experimental Study on the Strength and Crack Healing Performance of *E. coli* Bacteria-Induced Microbial Concrete. *Adv. Civ. Eng.* **2022**, *2022*, 3060230. [\[CrossRef\]](#)
19. Mangan, N.M.; Brenner, M.P. Systems analysis of the CO₂ concentrating mechanism in cyanobacteria. *eLife* **2014**, *3*, e02043. [\[CrossRef\]](#)
20. Durall, C.; Lindblad, P. Mechanisms of carbon fixation and engineering for increased carbon fixation in cyanobacteria. *Algal Res.* **2015**, *11*, 263–270. [\[CrossRef\]](#)
21. Hoffmann, T.D.; Reeksting, B.J.; Gebhard, S. Bacteria-induced mineral precipitation: A mechanistic review. *Microbiology* **2021**, *167*, 001049. [\[CrossRef\]](#) [\[PubMed\]](#)
22. Wu, Y.; Li, H.; Li, Y. Biomineralization Induced by Cells of *Sporosarcina pasteurii*: Mechanisms, Applications and Challenges. *Microorganisms* **2021**, *9*, 2396. [\[CrossRef\]](#) [\[PubMed\]](#)
23. Chuo, S.C.; Mohamed, S.F.; Mohd Setapar, S.H.; Ahmad, A.; Jawaid, M.; Wani, W.A.; Yaqoob, A.A.; Mohamad Ibrahim, M.N. Insights into the Current Trends in the Utilization of Bacteria for Microbially Induced Calcium Carbonate Precipitation. *Materials* **2020**, *13*, 4993. [\[CrossRef\]](#)
24. Tan, K.; Wu, S.; Ding, S. Carriers of Healing Agents in Biological Self-Healing Concrete. *Adv. Mater. Sci. Eng.* **2023**, *2023*, 7179162. [\[CrossRef\]](#)
25. Xu, J.; Wang, X.; Yao, W.; Kulminkaya, A.A.; Shah, S.P. Microbial-inspired self-healing of concrete cracks by sodium silicate-coated recycled concrete aggregates served as bacterial carrier. *Front. Struct. Civ. Eng.* **2024**, *18*, 14–29. [\[CrossRef\]](#)
26. Kim, H.; Son, H. Utilization of Bio-Mineral Carbonation for Enhancing CO₂ Sequestration and Mechanical Properties in Cementitious Materials. *Buildings* **2022**, *12*, 744. [\[CrossRef\]](#)
27. Yu, X.; Zhang, Q.; Zhang, X.; Luo, M. Microbial self-healing of cracks in cement-based materials and its influencing factors. *Front. Struct. Civ. Eng.* **2023**, *17*, 1630–1642. [\[CrossRef\]](#)

28. Demo, P.; Přeučil, F.; Prošek, Z.; Tichá, P.; Domonkos, M. Self-Healing of Cementitious Materials via Bacteria: A Theoretical Study. *Crystals* **2022**, *12*, 920. [\[CrossRef\]](#)
29. Bandlamudi, R.K.; Kar, A.; Ray Dutta, J. A review of durability improvement in concrete due to bacterial inclusions. *Front. Built Environ.* **2023**, *9*, 1095949. [\[CrossRef\]](#)
30. Ramagiri, K.K.; Chintha, R.; Bandlamudi, R.K.; Kara De Maeijer, P.; Kar, A. Cradle-to-Gate Life Cycle and Economic Assessment of Sustainable Concrete Mixes—Alkali-Activated Concrete (AAC) and Bacterial Concrete (BC). *Infrastructures* **2021**, *6*, 104. [\[CrossRef\]](#)
31. Al-Gheethi, A.A.; Memon, Z.A.; Balasbaneh, A.T.; Al-Kutti, W.A.; Mokhtar, N.; Othman, N.; Juki, M.I.; Noman, E.A.; Algaifi, H.A. Critical Analysis for Life Cycle Assessment of Bio-Cementitious Materials Production and Sustainable Solutions. *Sustainability* **2022**, *14*, 1920. [\[CrossRef\]](#)
32. Garces, J.I.T.; Dollente, I.J.; Beltran, A.B.; Tan, R.R.; Promentilla, M.A.B. Life cycle assessment of self-healing geopolymer concrete. *Clean. Eng. Technol.* **2021**, *4*, 100147. [\[CrossRef\]](#)
33. Jansson, C.; Northen, T. Calcifying cyanobacteria—The potential of biomineralization for carbon capture and storage. *Curr. Opin. Biotechnol.* **2010**, *21*, 365–371. [\[CrossRef\]](#) [\[PubMed\]](#)
34. Lamérand, C.; Shirokova, L.S.; Bénézech, P.; Rols, J.-L.; Pokrovsky, O.S. Carbon sequestration potential of Mg carbonate and silicate biomineralization in the presence of cyanobacterium *Synechococcus*. *Chem. Geol.* **2022**, *599*, 120854. [\[CrossRef\]](#)
35. Kamennaya, N.A.; Ajo-Franklin, C.M.; Northen, T.; Jansson, C. Cyanobacteria as Biocatalysts for Carbonate Mineralization. *Minerals* **2012**, *2*, 338–364. [\[CrossRef\]](#)
36. Wilcox, S.M.; Mulligan, C.N.; Neculita, C.M. Mineral Carbonation for Carbon Sequestration: A Case for MCP and MICP. *Int. J. Mol. Sci.* **2025**, *26*, 2230. [\[CrossRef\]](#)
37. Goodchild-Michelman, I.M.; Church, G.M.; Schubert, M.G.; Tang, T.-C. Light and carbon: Synthetic biology toward new cyanobacteria-based living biomaterials. *Mater. Today Bio* **2023**, *19*, 100583. [\[CrossRef\]](#)
38. Kazemian, M.; Shafei, B. Carbon sequestration and storage in concrete: A state-of-the-art review of compositions, methods, and developments. *J. CO₂ Util.* **2023**, *70*, 102443. [\[CrossRef\]](#)
39. Gupta, S.; Kua, H.W.; Pang, S.D. Healing cement mortar by immobilization of bacteria in biochar: An integrated approach of self-healing and carbon sequestration. *Cem. Concr. Compos.* **2018**, *86*, 238–254. [\[CrossRef\]](#)
40. Taharia, M.; Dey, D.; Das, K.; Sukul, U.; Chen, J.-S.; Banerjee, P.; Dey, G.; Sharma, R.K.; Lin, P.-Y.; Chen, C.-Y. Microbial induced carbonate precipitation for remediation of heavy metals, ions and radioactive elements: A comprehensive exploration of prospective applications in water and soil treatment. *Ecotoxicol. Environ. Saf.* **2024**, *271*, 115990. [\[CrossRef\]](#)
41. Fahimzadeh, M.; Pasbakhsh, P.; Mae, L.S.; Tan, J.B.L.; Raman, R.K.S. Multifunctional, Sustainable, and Biological Non-Ureolytic Self-Healing Systems for Cement-Based Materials. *Engineering* **2022**, *13*, 217–237. [\[CrossRef\]](#)
42. Nežerka, V.; Holeček, P.; Somr, M.; Tichá, P.; Domonkos, M.; Stiborová, H. On the Possibility of Using Bacteria for Recycling Finest Fractions of Concrete Waste: A Critical Review. *Rev. Environ. Sci. Biotechnol.* **2023**, *22*, 1–24. [\[CrossRef\]](#)
43. Bandyopadhyay, A.; Saha, A.; Ghosh, D.; Dam, B.; Samanta, A.K.; Dutta, S. Microbial Repairing of Concrete & Its Role in CO₂ Sequestration: A Critical Review. *Beni-Suef Univ. J. Basic Appl. Sci.* **2023**, *12*, 7. [\[CrossRef\]](#)
44. Saxena, A.; Abraham, A.; Sang, B.-I. Bio-Concrete for the Modern Era: Paving the Way for Future Construction. *J. Ceram. Process. Res.* **2024**, *25*, 1122–1141. [\[CrossRef\]](#)
45. Elgendy, I.M.; Elkaliny, N.E.; Saleh, H.M.; Darwish, G.O.; Almostafa, M.M.; Metwally, K.; Yahya, G.; Mahmoud, Y.A.-G. Bacteria-Powered Self-Healing Concrete: Breakthroughs, Challenges, and Future Prospects. *J. Ind. Microbiol. Biotechnol.* **2025**, *52*, kuae051. [\[CrossRef\]](#)
46. Wang, J.; Ersan, Y.C.; Boon, N.; De Belie, N. Application of Microorganisms in Concrete: A Promising Sustainable Strategy to Improve Concrete Durability. *Appl. Microbiol. Biotechnol.* **2016**, *100*, 2993–3007. [\[CrossRef\]](#)
47. Andalib, R.; Abd Majid, M.Z.; Hussin, M.W.; Ponraj, M.; Keyvanfar, A.; Mirza, J.; Lee, H.-S. Optimum Concentration of *Bacillus megaterium* for Strengthening Structural Concrete. *Constr. Build. Mater.* **2016**, *118*, 180–193. [\[CrossRef\]](#)
48. D'Costa, S.S. Mechanism of Biotransformation of Phosphogypsum by Urease and Carbonic Anhydrase Produced by *Lysinibacillus sphaericus*. Master's Thesis, Goa University, Panaji, India, 2023.
49. Okyay, T.O. Carbon Dioxide Sequestration Through Microbially-Induced Calcium Carbonate Precipitation Using Ureolytic Environmental Microorganisms. Available online: <https://uh-ir.tdl.org/server/api/core/bitstreams/9dfd05bb-9ff7-4c25-a785-1cd8e175c540/content> (accessed on 4 June 2025).
50. Zhu, X.; Mignon, A.; Nielsen, S.D.; Zieger, S.E.; Koren, K.; Boon, N.; De Belie, N. Viability determination of *Bacillus sphaericus* after encapsulation in hydrogel for self-healing concrete via microcalorimetry and in situ oxygen concentration measurements. *Cem. Concr. Compos.* **2021**, *119*, 104006. [\[CrossRef\]](#)
51. Chuenchom, C.; Intarasoontorn, J.; Sorasitthyanukarn, F.N.; Chindasiriphan, P.; Jongvivatsakul, P.; Thai boonrod, S.; Likitler-suang, S.; Pungrasmi, W.; Rojsitthisak, P. Enhancing concrete self-healing capabilities of *Bacillus sphaericus* spores through the encapsulation in biopolymeric microcapsules. *J. Sustain. Cem.-Based Mater.* **2024**, *13*, 1582–1595. [\[CrossRef\]](#)

52. Luhar, S.; Luhar, I.; Shaikh, F.U.A. A Review on the Performance Evaluation of Autonomous Self-Healing Bacterial Concrete: Mechanisms, Strength, Durability, and Microstructural Properties. *J. Compos. Sci.* **2022**, *6*, 23. [CrossRef]
53. Xu, J.; Wang, X. Self-healing of concrete cracks by use of bacteria-containing low alkali cementitious material. *Constr. Build. Mater.* **2018**, *167*, 1–14. [CrossRef]
54. Khaliq, W.; Ehsan, M.B. Crack healing in concrete using various bio influenced self-healing techniques. *Constr. Build. Mater.* **2016**, *102*, 349–357. [CrossRef]
55. Ivaškė, A.; Gribniak, V.; Jakubovskis, R.; Urbonavičius, J. Bacterial Viability in Self-Healing Concrete: A Case Study of Non-Ureolytic *Bacillus* Species. *Microorganisms* **2023**, *11*, 2402. [CrossRef] [PubMed]
56. Fahimzadeh, M.; Abeyratne, A.; Mae, L.; Singh, R.; Pasbakhsh, P. Biological Self-Healing of Cement Paste and Mortar by Non-Ureolytic Bacteria Encapsulated in Alginate Hydrogel Capsules. *Materials* **2020**, *13*, 3711. [CrossRef]
57. González, L.M.; Mukhitov, N.; Voigt, C.A. Resilient living materials built by printing bacterial spores. *Nat. Chem. Biol.* **2020**, *16*, 126–133. [CrossRef]
58. Thongchom, C.; Laemthong, T.; Sangkeaw, P.; Yamasmit, N.; Keawsawasvong, S. Evaluation of encapsulated *Bacillus subtilis* bio-mortars for use under acidic conditions. *Sci. Rep.* **2024**, *14*, 25947. [CrossRef]
59. Adilah, R.N.; Chiu, S.-T.; Hu, S.-Y.; Ballantyne, R.; Happy, N.; Cheng, A.-C.; Liu, C.-H. Improvement in the probiotic efficacy of *Bacillus subtilis* E20-stimulates growth and health status of white shrimp, *Litopenaeus vannamei* via encapsulation in alginate and coated with chitosan. *Fish Shellfish Immunol.* **2022**, *125*, 74–83. [CrossRef]
60. Bolan, S.; Hou, D.; Wang, L.; Hale, L.; Egamberdieva, D.; Tammeorg, P.; Li, R.; Wang, B.; Xu, J.; Wang, T.; et al. The potential of biochar as a microbial carrier for agricultural and environmental applications. *Sci. Total Environ.* **2023**, *886*, 163968. [CrossRef]
61. Aytekin, B.; Mardani, A.; Yazıcı, Ş. State-of-art review of bacteria-based self-healing concrete: Biomineralization process, crack healing, and mechanical properties. *Constr. Build. Mater.* **2023**, *378*, 131198. [CrossRef]
62. Mohammed, H.; Ortoneda-Pedrola, M.; Nakouti, I.; Bras, A. Experimental characterisation of non-encapsulated bio-based concrete with self-healing capacity. *Constr. Build. Mater.* **2020**, *256*, 119411. [CrossRef]
63. Maqbool, S.; Singh, K. Effect of bacterial encapsulation in concrete: A review on applications and effects. *Mater. Today Proc.* **2020**, *33*, 1713–1719. [CrossRef]
64. Yaqoob Wani, I.; Singh, K. Effect of encapsulated bacteria on concrete properties: A review. *Mater. Today Proc.* **2020**, *33*, 1706–1712. [CrossRef]
65. Vedrtam, A.; Palou, M.T.; Varela, H.; Gunwant, D.; Kalauni, K.; Barluenga, G. Experimental and numerical study on post-fire self-healing concrete for enhanced durability. *Sci. Rep.* **2025**, *15*, 9731. [CrossRef]
66. Vedrtam, A.; Gunwant, D.; Kalauni, K.; Palou, M.T. Experimental and numerical study on sustainable post-fire repair of concrete structures using bacterial self-healing mechanisms. *Constr. Build. Mater.* **2025**, *474*, 141175. [CrossRef]
67. Zadeike, D.; Gaizauskaite, Z.; Basinskiene, L.; Zvirdauskiene, R.; Cizeikiene, D. Exploring Calcium Alginate-Based Gels for Encapsulation of *Lactocaseibacillus paracasei* to Enhance Stability in Functional Breadmaking. *Gels* **2024**, *10*, 641. [CrossRef]
68. Klikova, K.; Holecek, P.; Nezerka, V.; Prosek, Z.; Konakova, D.; Demnerova, K.; Stiborova, H. Application of *Sporosarcina pasteurii* for the biomineralization of calcite in the treatment of waste concrete fines. *Environ. Sci. Pollut. Res.* **2025**. [CrossRef]
69. Wani, S.; Jan Geça, M.; Selvaraj, T.; Shanmuga Priya, T. Assessing the influence of *Bacillus megaterium* and *Bacillus sphaericus* in cementitious materials: Promoting sustainability towards strength, durability and crack repair. *Ain Shams Eng. J.* **2024**, *15*, 102748. [CrossRef]
70. Kliková, K.; Holeček, P.; Koňáková, D.; Stiborová, H.; Nežerka, V. Exploiting *Bacillus pseudofirmus* and *Bacillus cohnii* to promote CaCO₃ and Aft phase formation for stabilizing waste concrete fines. *Cem. Concr. Compos.* **2025**, *155*, 105839. [CrossRef]
71. Zhan, Q.; Zhou, J.; Wang, S.; Su, Y.; Liu, B.; Yu, X.; Pan, Z.; Qian, C. Crack self-healing of cement-based materials by microorganisms immobilized in expanded vermiculite. *Constr. Build. Mater.* **2021**, *272*, 121610. [CrossRef]
72. Srinivas M, K.; Alengaram, U.J.; Ibrahim, S.; Phang, S.M.; Vello, V.; Jun, H.K.; Alnahhal, A.M. Evaluation of crack healing potential of cement mortar incorporated with blue-green microalgae. *J. Build. Eng.* **2021**, *44*, 102958. [CrossRef]
73. ISO 14040; Life Cycle Assessment. ISO: Geneva, Switzerland, 2006.
74. ISO 14044; Environmental Management—Life Cycle Assessment—Requirements and Guidelines. ISO: Geneva, Switzerland, 2006.
75. Ecoinvent Version 3.8. Available online: <https://support.ecoinvent.org/ecoinvent-version-3.8> (accessed on 30 May 2025).
76. OpenLCA.org | OpenLCA is a Free, Professional Life Cycle Assessment (LCA) and Footprint Software with a Broad Range of Features and Many Available Databases, Created by GreenDelta Since 2006. Available online: <https://www.openlca.org/> (accessed on 4 May 2025).
77. SimaPro-Sustainability Insights for Informed Changemakers. Available online: <https://simapro.com/> (accessed on 30 May 2025).
78. Justo-Reinoso, I.; Arena, N.; Reeksting, B.J.; Gebhard, S.; Paine, K. Bacteria-based self-healing concrete—A life cycle assessment perspective. *Dev. Built Environ.* **2023**, *16*, 100244. [CrossRef]

79. *ACI 318; Building Code Requirements for Structural Concrete and Commentary*. American Concrete Institute: Farmington Hills, MI, USA, 2022.
80. *EN 1992-1-1; Eurocode 2: Design of Concrete Structures—Part 1-1: General Rules and Rules for Buildings*. The European Union Per Regulation: Brussels, Belgium, 2004.
81. *ASTM C150; Standard Specification for Portland Cement*. ASTM International: West Conshohocken, PA, USA, 2012.
82. *ISO 50500; Innovation Management*. ISO: Geneva, Switzerland, 2017.

Disclaimer/Publisher’s Note: The statements, opinions and data contained in all publications are solely those of the individual author(s) and contributor(s) and not of MDPI and/or the editor(s). MDPI and/or the editor(s) disclaim responsibility for any injury to people or property resulting from any ideas, methods, instructions or products referred to in the content.